LOS ALAMOS SCIENTIFIC LABORATORY
OF THE UNIVERSITY OF CALIFORNIA o LOS ALAMOS NEW MEXICO

TWO-DIMENSIONAL HYDRODYNAMIC CALCULATIONS

Sept 59

LEGAL NOTICE

Printed in USA. Price $2.50. Available from the

Office of Technical Services
U. S. Department of Commerce
Washington 25, D. C.

LA-2301
PHYSICS AND MATHEMATICS
TID-4500 (14th ed.)

LOS ALAMOS SCIENTIFIC LABORATORY
OF THE UNIVERSITY OF CALIFORNIA LOS ALAMOS NEW MEXICO

REPORT WRITTEN: April 1959

REPORT DISTRIBUTED: September 23, 1959

TWO-DIMENSIONAL HYDRODYNAMIC CALCULATIONS

by

Francis H. Harlow

with

Donald O. Dickman (Chapters II, III, IV, V)
David E. Harris, Jr. (Chapter VI)
Robert E. Martin (Chapters VI, VII)

Contract W-7405-ENG. 36 with the U. S. Atomic Energy Commission

ABSTRACT

Previous discussions of a computing method for solving two-dimensional hydrodynamic problems are here amplified and extended. Results of computations are presented for problems involving shock diffraction and refraction, surface instabilities, and viscous flow.

TABLE OF CONTENTS

INTRODUCTION

The particle-in-cell method for two-dimensional hydrodynamic calculations has been applied with various degrees of success to a rather wide variety of problems in compressible-fluid flow. The method was first discussed in two unpublished reports[1,2] which have been superseded by more detailed published descriptions of the method and its characteristics.[3,4] The most complete description previously could be found in Ref. 4. That discussion was mainly restricted to one-dimensional procedures, however, and as applied to two-dimensional calculations was incomplete and should now be modified somewhat. It is, therefore, one purpose of this report to discuss the presently used procedure in some detail.

The accuracy of the computing method has been tested by applying it to a variety of problems for which theoretical or experimental solutions were available. The results of some of these calculations have been reported;[5,6,7] others are available only in classified literature. Still others, more recently obtained, have revealed new restrictions, or regions of applicability, or have produced results not previously derived by theoretical methods. It is, therefore, the second purpose of this report to summarize these new results.

For brevity in writing, the particle-in-cell method for hydrodynamic calculations has been abbreviated the PIC method. In the discussions to follow, it will be assumed that the reader has access to Ref. 4 so that most of the discussions presented there will not be repeated. On the other hand, the outline of computing procedure in Chapter I of this report is sufficiently

complete in itself so that a computing code could be based on it.

Performance of a calculation by the PIC method resembles the performance of an experiment. In preparation, the differential equations of motion are transformed to suitable conservative finite-difference forms. These, together with the initial and boundary conditions for a specific situation, are given to the electronic computer which, in turn, develops the solution at a sequence of later times separated by small time increments. There is no a priori assumption of a model for the flow configuration; the development of shocks, for example, occurs automatically where required. Thus, these computations are quite different from another type often performed by high-speed computers, in which a complicated set of equations is solved very precisely, often for the purpose of normalizing analytical approximation procedures. Precise solutions, however, are usually possible only with ordinary differential equations. In contrast, the PIC method approach for solving the partial differential equations of hydrodynamic always results in approximate solutions. It has been observed but not proved that under many circumstances of interest the approximations are good and, furthermore, that they can be improved by decreasing the sizes of the finite-difference zones.

In the absence of analytical justifications of the PIC methodology, it has been necessary to examine by "trial and error" its applicability to numerous problems with known solutions. Likewise, it has been necessary to experiment with numerous modifications of the methodology in order to obtain maximum accuracy with the resolution presently obtainable with available computing machines. In some cases, it has been found that a modification would result in very little change in the answer; in other cases, a small change could produce a very large effect. Some of these results are discussed in this report.

The calculation method is designed for use with a large high-speed

computer. All calculations described in this report were performed on an IBM Electronic Data Processing Machine, type 704, with 32K memory.

The results discussed in each chapter were assembled mainly by the people mentioned on the title page. There were, however, many occasions when techniques discovered in the preparation of one computing code were applied to another, so that contributions from all of the authors can be found throughout the report. In addition, contributions to these later developments in the PIC methodology have been made by Martha W. Evans and Billy D. Meixner. Many stimulating discussions with them have resulted in significant contributions to this report; details of their recent studies are to be reported elsewhere.

CHAPTER I

THE CALCULATION PROCEDURE

A. Problems Involving Cartesian Coordinates in a Rigid Rectangular Box

1. Layout and Nomenclature. Two materials are confined to move in a two-dimensional rectangular box whose walls are rigid and allow perfect slippage. The materials are nonviscous and nonconducting of heat; each has an equation of state which relates pressure, p, to density, ρ, and specific internal energy, I.

The box is oriented with one corner at the origin and with the edges along the x and y axes. It is subdivided into a number of equal rectangular cells to which the finite-difference equations are to be related. The cells have dimensions δx and δy, whose ratio is not necessarily the same as the ratio of lengths of the box sides. A typical layout is shown.

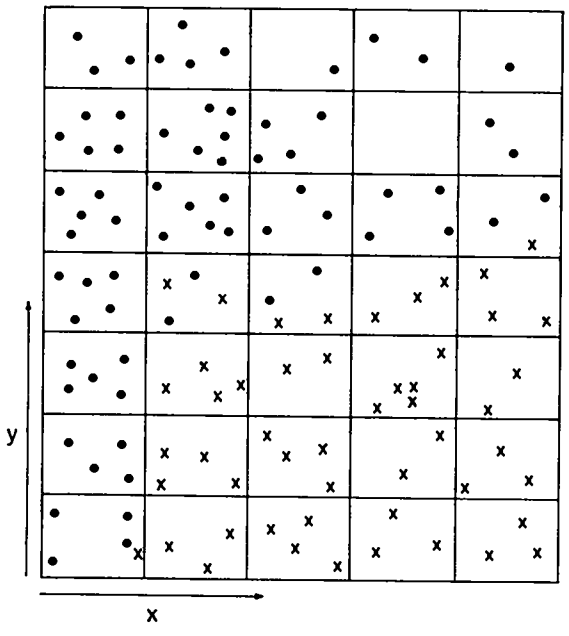

Each fluid is represented by a number of mass points called "particles," each with a constant mass; as shown in the figure, these are represented by dots and x's; we shall

call the materials "dot material" and "x material," respectively. In this example, all dot particles have the same mass, $m_{\cdot}$, and all the x particles have the same mass, m_x. (For calculations in cylindrical coordinates or for certain situations in cartesian coordinates, it is more convenient to have a different mass for every particle.) For each particle there are stored in the machine memory its x and y coordinates. These are changed in time, by the method described below, to give a representation of the motion of the fluids through the mesh of cells.

Such quantities as velocity, density, and pressure are kept in the machine memory by cell, so that, for example, the pressure of a cell is a certain average of the pressure throughout the cell. (Further discussion of this point is given by Bromberg in Appendix II of Ref. 4, where there is an enlightening alternative derivation of the PIC method equations.) The cells are labeled with index $\binom{j}{i}$, with i and j increasing in the x and y directions, respectively; the lower left cell in the figure is cell number $\binom{1}{1}$. The pressure for cell $\binom{j}{i}$ is p^j_i, while the average pressure along the boundary between cells $\binom{j}{i}$ and $\binom{j}{i+1}$ is $p^j_{i+\frac{1}{2}}$; analogous symbols are used for the other boundary pressures. The density in a cell is defined to be the quotient of the sum of the masses in the cell divided by its area.

The nomenclature for various cellwise quantities is shown in Table I-1.

2. The Pressures. The two equations of state are given in the form

$$p = f_{\cdot}(\rho, I)$$

$$p = f_x(\rho, I)$$

where $f_{\cdot}$ and f_x are appropriate functions for the dot and x materials, respectively. For a cell containing only dot or x material, these equations become

TABLE I-1

IDENTITY OF NOMENCLATURE FOR CELL $\binom{j}{i}$

$u_i^j \equiv$ x-direction component of velocity

$v_i^j \equiv$ y-direction component of velocity

$M_{\cdot i}^j \equiv$ mass of dot material $\left(\equiv N_{\cdot i}^j m_{\cdot}\right)$

$M_{x_i}^j \equiv$ mass of x material $\left(\equiv N_{x_i}^j m_x\right)$

$M_i^j \equiv M_{x_i}^j + M_{\cdot i}^j$

$I_{\cdot i}^j \equiv$ specific internal energy of dot material

$I_{x_i}^j \equiv$ specific internal energy of x material

$p_i^j \equiv$ pressure

$\delta Q_i^j \equiv$ the Phase I change in total internal energy

$E_{\cdot i}^j \equiv$ total energy of dot material

$E_{x_i}^j \equiv$ total energy of x material

$X_i^j \equiv$ total x-direction momentum

$Y_i^j \equiv$ total y-direction momentum

$\tilde{(\,)} \equiv$ result of Phase I calculation for ( )

$(\,)' \equiv$ result of Phase II calculation for ( )

$$p_i^j = f_{\cdot}\left[\frac{M_{\cdot i}^{\ j}}{\delta x \delta y},\ I_{\cdot i}^{\ j}\right]$$

$$p_i^j = f_x\left[\frac{M_{x_i}^{\ j}}{\delta x \delta y},\ I_{x_i}^{\ j}\right]$$

Various procedures are possible for the determination of total pressure in a mixed cell. One of these is based on the requirement of pressure continuity across a material interface. Assuming that the fraction of a cell occupied by dot material is σ, one writes the two equations, from which σ is to be eliminated,

$$p_i^j = f_{\cdot}\left[\frac{M_{\cdot i}^{\ j}}{\sigma \delta x \delta y},\ I_{\cdot i}^{\ j}\right] = f_x\left[\frac{M_{x_i}^{\ j}}{(1-\sigma)\delta x \delta y},\ I_{x_i}^{\ j}\right] \qquad (1)$$

If the pressure is strictly proportional to the density for both materials, then the result is the same as that from adding partial pressures:

$$p_i^j = f_{\cdot}\left[\frac{M_{\cdot i}^{\ j}}{\delta x \delta y},\ I_{\cdot i}^{\ j}\right] + f_x\left[\frac{M_{x_i}^{\ j}}{\delta x \delta y},\ I_{x_i}^{\ j}\right] \qquad (2)$$

If the equations of state are complicated, it may be convenient, as well as sufficiently accurate, to still calculate the pressure in a mixed cell by adding the partial pressures in this manner. In some cases, however, the result of this is far from reasonable and the use of Eq. (1) is indicated. An approximate solution of Eq. (1) has been found useful on several occasions. A value, σ_0, is assumed for σ and the pressure is taken to be

$$p_i^j = \frac{1}{2}\left\{ f_{\cdot}\left[\frac{M_{\cdot i}^{\ j}}{\sigma_0 \delta x \delta y},\ I_{\cdot i}^{\ j}\right] + f_x\left[\frac{M_{x_i}^{\ j}}{(1-\sigma_0)\delta x \delta y},\ I_{x_i}^{\ j}\right]\right\}$$

The choice of

$$\sigma_0 = \frac{M_{\cdot i}^{\ j}}{M_{\cdot i}^{\ j} + R M_{x_i}^{\ j}}$$

has sometimes yielded reasonable results, where R is the ratio of the initial density of the dot material to that of the x material. Thus, the value of σ_0 is based on the assumption that the compression of each of the two materials is in the same ratio as their initial compressions.

Various iterative procedures are possible for solving Eq. (1); none of these has been used.

3. Phase I of a Calculation Cycle. In the machine memory there are stored all the results of the previous-cycle calculations or else the initial conditions for the problem. These are to be advanced in time according to a finite-difference approximation to the differential equations

$$\frac{\partial \rho}{\partial t} + u\frac{\partial \rho}{\partial x} + v\frac{\partial \rho}{\partial y} + \rho\left(\frac{\partial u}{\partial x} + \frac{\partial v}{\partial y}\right) = 0$$

$$\rho\frac{\partial u}{\partial t} + \rho u\frac{\partial u}{\partial x} + \rho v\frac{\partial u}{\partial y} + \frac{\partial p}{\partial x} = 0$$

$$\rho\frac{\partial v}{\partial t} + \rho u\frac{\partial v}{\partial x} + \rho v\frac{\partial v}{\partial y} + \frac{\partial p}{\partial y} = 0$$

$$\rho\frac{\partial}{\partial t}\left[I + \frac{1}{2}\left(u^2 + v^2\right)\right] + \rho u\frac{\partial}{\partial x}\left[I + \frac{1}{2}\left(u^2 + v^2\right)\right] + \rho v\frac{\partial}{\partial y}\left[I + \frac{1}{2}\left(u^2 + v^2\right)\right] + \frac{\partial pu}{\partial x} + \frac{\partial pv}{\partial y} = 0$$

The first of these equations, that of mass conservation, is automatically satisfied by the particle model. The other three equations are treated as follows: In Phase I, the contributions to the time derivatives which arise from the terms involving pressure are calculated. The particles are not moved at this step; thus the transport terms are dropped, and the equations become, in finite space-difference form,

$$\rho_i^j \left(\frac{\partial u}{\partial t}\right)_i^j = -\frac{1}{\delta x}\left[p_{i+\frac{1}{2}}^j - p_{i-\frac{1}{2}}^j\right]$$

$$\rho_i^j \left(\frac{\partial v}{\partial t}\right)_i^j = -\frac{1}{\delta y}\left[p_i^{j+\frac{1}{2}} - p_i^{j-\frac{1}{2}}\right]$$

$$\rho_i^j \frac{\partial}{\partial t}\left[I + \frac{1}{2}\left(u^2 + v^2\right)\right]_i^j = -\frac{1}{\delta x}\left[(pu)_{i+\frac{1}{2}}^j - (pu)_{i-\frac{1}{2}}^j\right] - \frac{1}{\delta y}\left[(pv)_i^{j+\frac{1}{2}} - (pv)_i^{j-\frac{1}{2}}\right]$$

From these result the tentative new cellwise velocities

$$\tilde{u}_i^j = u_i^j - \frac{\delta y \delta t}{M_j^i}\left[p_{i+\frac{1}{2}}^j - p_{i-\frac{1}{2}}^j\right]$$

$$\tilde{v}_i^j = v_i^j - \frac{\delta x \delta t}{M_i^j}\left[p_i^{j+\frac{1}{2}} - p_i^{j-\frac{1}{2}}\right]$$

The quantity I_i^j in the third equation is not defined for a mixed cell, but we may write

$$\rho_i^j \frac{\partial I_i^j}{\partial t} \rightarrow \left(\frac{1}{\delta x \delta y}\right)\frac{\delta Q_i^j}{\delta t}$$

wherein δQ_i^j is the change in total internal energy of the cell. Its calculation involves use of the old and new velocities

$$\delta Q_i^j = \frac{1}{2} M_i^j \left[\left(u_i^j\right)^2 + \left(v_i^j\right)^2 - \left(\tilde{u}_i^j\right)^2 - \left(\tilde{v}_i^j\right)^2 \right] - \delta y \delta t \left[(pu)^j_{i+\frac{1}{2}} - (pu)^j_{i-\frac{1}{2}} \right]$$
$$- \delta x \delta t \left[(pv)_i^{j+\frac{1}{2}} - (pv)_i^{j-\frac{1}{2}} \right]$$

It is seen that the values of pressures and velocities at cell boundaries are required. The usual procedure in obtaining these has been as follows: Between two ordinary cells, the boundary pressure and velocity are taken as the averages of those quantities in the two adjacent cells. At the rigid box boundary, the normal velocity component is zero, while the tangential does not need specification. The pressure at the box boundary has been taken as a quadratic extrapolation of the pressures in the two adjacent cells. The quadratic extrapolation is used because it allows the requirement to be imposed that the normal derivative of the pressure vanish at the boundary. It is nearly as satisfactory to use for the boundary pressure that of the adjacent interior cell.

At the boundary between an ordinary cell and an interior empty one, the pressure is chosen to be zero so that the velocity there need not be specified. Such a choice ensures energy conservation.

It has been found to make little difference in the final results of a calculation whether one uses, in the energy equation, the product of average pressure and average velocity, or the average of the pressure-velocity product; most of our calculations have used the former.

From the result for δQ_i^j, the values of $\tilde{I}_{\cdot i}^{\,j}$ and $\tilde{I}_{x_i}^{\,j}$ are to be determined. For an unmixed cell with, say, dot material only,

$$\tilde{I}_{\cdot i}^{\,j} = I_{\cdot i}^{\,j} + \frac{\delta Q_i^j}{M_{\cdot i}^{\,j}}$$

One way of distributing internal energy in a mixed cell was described in Ref. 4 (page 21). The method more recently used is based on the assumption that both components are compressed or expanded adiabatically through the same pressure change.* For example, if both components are represented by polytropic equations of state

$$p_k = (\gamma_k - 1)\rho_k I_k$$

(where k means . or x), then

$$\tilde{I}_{kd}^{j} = I_{kd}^{j}\left\{1 + \frac{(\gamma_k - 1)\delta Q_1^j}{\gamma_k \sum_{k'}\left[\left(\frac{\gamma_{k'} - 1}{\gamma_{k'}}\right)M_{k'i}{}^{j}I_{k'i}{}^{j}\right]}\right\}$$

If the equations of state are more complicated, then the distribution may be based on other assumptions, such as (1) both components receive the same change in total internal energy, or (2) both components receive the same change in specific internal energy. Application of the first of these two procedures yielded good results in one trial calculation, whereas the results of using the second were not as good—insufficient energy was transferred across the boundary from a heavy material to a light one.

4. Phase II, The Transport of Material. By the end of Phase I, there are stored in memory ten quantities for every cell. Table I-2 shows these, together with the quantities which replace them during the sequence of Phase II calculations.

TABLE I-2

SEQUENCE OF STORAGE CHANGES FOR CELL$\binom{j}{i}$ DURING PHASE II

	$M_\cdot$	M_x	$I_\cdot$	I_x	$\tilde{I}_\cdot$	$\tilde{I}_x$	u	v	$\tilde{u}$	$\tilde{v}$
Step 1 >	"	"	$\tilde{E}_\cdot$	$\tilde{E}_x$	"	"	$\tilde{X}$	$\tilde{Y}$	"	"
Step 2 >	$M'_\cdot$	M'_x	$E'_\cdot$	E'_x	"	"	X'	Y'	"	"
Step 3 >	"	"	"	"	"	"	u'	v'	"	"
Step 4 >	"	"	$I'_\cdot$	I'_x	"	"	"	"	"	"

Step 1. The results of the Phase I calculations are transformed into total cellwise energies and momenta:

$$\tilde{E}_\cdot \equiv M_\cdot\left[\tilde{I}_\cdot + \frac{1}{2}\left(\tilde{u}^2 + \tilde{v}^2\right)\right]$$

$$\tilde{E}_x \equiv M_x\left[\tilde{I}_x + \frac{1}{2}\left(\tilde{u}^2 + \tilde{v}^2\right)\right]$$

$$\tilde{X} \equiv \left(M_\cdot + M_x\right)\tilde{u}$$

$$\tilde{Y} \equiv \left(M_\cdot + M_x\right)\tilde{v}$$

Step 2. The particles are moved. The coordinates of each change according to

$$x' = x + \bar{u}\delta t$$

$$y' = y + \bar{v}\delta t$$

In some calculations (see, for example, Ref. 7), the values of $\bar{u}$ and $\bar{v}$ were simply the values of $\tilde{u}$ and $\tilde{v}$ of the cell containing the particle, no matter where in the cell the particle originated its motion for the cycle. The results can almost always be improved, however, by using the time-consuming

process called "velocity weighting;" in fact, tests have indicated that the increase in accuracy thereby realized could not be achieved by that increase in mesh fineness which would consume equal extra time.

In the velocity weighting procedure, a rectangle of cell size is imagined to be located about each particle, the particle being at the center. Such a rectangle then overlaps four adjacent cells, and the effective velocity for moving the particle is taken as a weighted average of the four cellwise velocities, the weightings being proportional to the overlap areas. If the surrounding rectangle lies partly in an empty cell, then that cell may be assumed to have the same velocity as does the cell with the particle (or any other convenient and reasonable velocity) for the purpose of determining the effective velocity for movement. If the surrounding rectangle lies outside the walls of the computation region, then the fictitious outside cells may be given either reflected velocities or the same velocities as in the adjacent interior cells. In the former case, it may be shown that for properly small values of δt, no particle will be lost from the system. The procedure is less desirable, however, as it can lead to the "boundary catastrophe" discussed in Ref. 4 (page 17). In the latter case, it is necessary to reflect the particle back in; the particle then carries a change in momentum as though entering from a cell with reflected velocity, and the boundary catastrophe is avoided.

When a particle is thus moved, it may be found to remain in the same cell from which it started. In this case, there is no modification to any of the cellwise quantities. Some of the particles, however, will end up in new cells; in these cases, cellwise changes are necessary. From the cell which was left, the particle mass, momentum, and energy are subtracted and these are added to the new cell. Thus, through step 2, the cellwise values of mass, momentum, and energy cumulate to their final values for the cycle.

Step 3. The final velocities for the cycle are computed

$$u' = \frac{X'}{M'_{\cdot} + M'_{x}}$$

$$v' = \frac{Y'}{M'_{\cdot} + M'_{x}}$$

Step 4. The final specific internal energies for the cycle are computed

$$I'_{\cdot} = \frac{E'_{\cdot}}{M'_{\cdot}} - \frac{1}{2}\left[(u')^2 + (v')^2\right]$$

$$I'_{x} = \frac{E'_{x}}{M'_{x}} - \frac{1}{2}\left[(u')^2 + (v')^2\right]$$

5. Phase III, Functionals of Motion. The final arrangement of storage after the sequence of calculations is such as to allow immediate re-entry into Phase I of the next cycle. Ordinarily, however, before proceeding to the next cycle, it is useful to compute various functionals of the motion such as total kinetic and internal energy for each material, components of total momentum, positions of centers of mass, entropy, and numerous other quantities. In some cases, it is possible to compare changes of these quantities with the changes calculated by summing boundary fluxes. Thus, in the example at hand, the total energy of the system should be rigorously conserved. (Actually, machine roundoff will introduce some change in total energy, but the relative change per cycle should be bounded by a number which is predictable from a knowledge of the number of significant figures retained by the calculation.) Likewise, changes in the momentum components should be exactly predictable in terms of the sum of the boundary forces. Computed by machine, such checks serve to indicate machine or coding errors and have proved extremely valuable on many occasions.

B. Other Boundary Conditions in Cartesian Coordinates

The simple boundary conditions discussed in the previous section are applicable only to a restricted class of problems. Various modifications are listed below; most of them have been used in actual calculations.

1. Periodic Channel. The rectangular computation region can be considered to be one section of an infinite channel with walls parallel to, say, the x axis. It is assumed that all properties of the entire flow field are periodic along the channel, the period being the width of the computation region. The change in computing procedure is slight. For example, along the right-hand boundary, the cells are treated just like interior cells with their right-hand neighbors being the cells along the left-hand boundary. Particles leaving the system across the boundary re-enter from the left, while those which go out the left-hand boundary are inserted from the right. The condition of periodicity is applied in such a way that the positions of the vertical boundaries are immaterial as long as they are separated by one period. Such a system is completely conservative of particles, energy, and horizontal momentum. This type of system was used in performing the calculations discussed in Chapters V and VII.

2. Prescribed Input. Along one or several of the boundaries, a prescribed input of fluid can be inserted. This could, for example, be used to represent the flow conditions behind a shock which has entered across one of the boundaries at the beginning of the problem. Consider the example of input along the left boundary. The left-hand cells of the computation region can be treated as interior cells with their left-hand neighbors being considered to possess the prescribed conditions of the input flow. Particles are periodically "created" for insertion across the left boundary; there is thus a slight additional bookkeeping difficulty with regard to the storage of

particle coordinates. This type of input system has been used in numerous calculations, including those discussed in Chapters II, III, and IV, and in Refs. 5 and 7.

3. Continuative Output. Whenever the input boundary condition (paragraph 2 above) is used, a provision for output at some other boundary is usually required. If the flow out of that boundary is supersonic, then the exact manner by which it is treated is of little importance. We have always used a "continuative" boundary treatment for such an output line. Accordingly, the boundary cells are treated as interior, being bounded on the outside by cells with identically the same properties, at any instant, as their adjacent interior neighbors. The machine memory locations for storage of the coordinates of lost particles are made available for incoming particles, so that the total required machine memory is bounded, and a calculation can be continued indefinitely.

4. Moving Mesh. In paragraphs 1, 2, and 3 above, the computation region is at rest and the fluid streams by. Alternately, if it is desirable to study some feature of the flow moving with fluid speed (or some other speed), it could be possible to have a traveling region of computation. Suppose, for example, one wished to follow the motion of a shock wave during its passage down a channel in, say, the x direction. This could be accomplished as follows. A zone of several cells would always be present ahead of the shock; whenever the shock had advanced a cell width, a new column of cells would be created to their right with conditions representing the initial state ahead of the shock. At the same time, a column of cells downstream would be destroyed. Conditions ahead of the shock could be constant or could vary with space. Boundary conditions at the downstream boundary could be continuative. No calculations have been reported which used a moving computation region in this manner.

5. Rigid Obstacle. A rigid obstacle can be placed within the computation region. This is most easily accomplished if the boundaries of the obstacle follow cell boundaries. The treatment is then exactly the same as at the rigid walls of the computation region. Such a calculation was reported in Ref. 5. If the obstacle boundary is curved or oblique relative to the cell orientation, then the procedure is somewhat more complicated. Numerous partial cells are created. The finite-difference equations for such cells can be derived from the integral form of the equations of motion by a procedure like that used by Bromberg (Ref. 4, Appendix II) for deriving the equations under ordinary circumstances. The results of calculations for flow past a circular object were reported in Ref. 7.

6. Applied Pressure. An applied pressure, prescribed as a function of space and time, can be exerted on the irregular surface of a fluid. We have accomplished this by varying the empty cell treatment, using the empty cells to signal the presence of an applied pressure. First, the motion of particles is subjected to an additional constraint: If the motion of any particle results in emptying a cell, then the particle is not allowed to move during that cycle. An exception is allowed if the emptying cell is adjacent to one which is already empty. Initially, the fluid interior has no empty cells; the region of applied pressure is an empty-cell region surrounding the fluid. In most of our problems the resulting motion is compressive, so that the constraint by which no interior cells may empty is not serious. The boundary of every fluid cell adjacent to an empty cell is given the appropriate applied pressure, and it is assumed that the velocity at that boundary is that of the fluid cell. The pressure within a cell next to an empty one is calculated using normal density in the equation of state, if the cell would otherwise have subnormal density. In all other cases these edge cells are treated as ordinary interior cells. This procedure has been used in the

calculations reported in Chapter VI and in other calculations not reported.

An interpretation of the applied pressure boundary condition is as follows. The "empty" cells behave as though they were filled with a gas whose density is very small compared with that of the adjacent material, but whose temperature is very high in such a way that the pressure is finite (the prescribed value). As a result the sound speed is very high so that the pressure remains homogeneous.

C. Generalized Problems in Cartesian Coordinates

If there is an applied body force, or if the fluids are viscous and conducting of heat, then the equations and boundary conditions become somewhat more complicated, but the basic method is not altered. As an example, consider the problem of determining the nonsteady motion of a polytropic gas flowing through a periodic two-dimensional channel bounded by walls parallel to the x axis. The basic equations (in addition to that of mass conservation, which is still identically satisfied) are

$$\rho \frac{du}{dt} = \rho g + \frac{\partial}{\partial x}\left(P + 2\mu \frac{\partial u}{\partial x}\right) + \frac{\partial Q}{\partial y}$$

$$\rho \frac{dv}{dt} = \frac{\partial}{\partial y}\left(P + 2\mu \frac{\partial v}{\partial y}\right) + \frac{\partial Q}{\partial x}$$

$$\rho \frac{d}{dt}\left[I + \frac{1}{2}\left(u^2 + v^2\right)\right] = \rho u g + \frac{\partial}{\partial x}\left[Pu + Qv + \mu \frac{\partial}{\partial x}\left(BI + u^2\right)\right]$$

$$+ \frac{\partial}{\partial y}\left[Pv + Qu + \mu \frac{\partial}{\partial y}\left(BI + v^2\right)\right]$$

where the additional symbols are

$$P \equiv -p + \mu A\left(\frac{\partial u}{\partial x} + \frac{\partial v}{\partial y}\right)$$

$$Q \equiv \mu\left(\frac{\partial v}{\partial x} + \frac{\partial u}{\partial y}\right)$$

$\mu \equiv$ first (ordinary) viscosity coefficient

$\lambda \equiv$ second viscosity coefficient

$A \equiv \lambda/\mu$ (assumed constant; an idealized monatomic gas has $A = -\frac{2}{3}$)

$\gamma \equiv$ ratio of specific heats (assumed constant)

$P_r \equiv$ Prandtl number (assumed constant)

$B \equiv \gamma/P_r$ [a relatively simple theoretical model gives $B = \frac{1}{4}(9\gamma - 5)$]

$g \equiv$ acceleration of body force (exerted in the x direction only)

Transformation of the equations to finite-difference form proceeds as before. For Phase I of the calculation

$$\tilde{u}_i^j = u_i^j + g\delta t + \frac{\delta y \delta t}{M_i^j}\left\{P_{i+\frac{1}{2}}^j - P_{i-\frac{1}{2}}^j + \frac{2}{\delta x}\left[\mu_{i+\frac{1}{2}}^j\left(u_{i+1}^j - u_i^j\right) - \mu_{i-\frac{1}{2}}^j\left(u_i^j - u_{i-1}^j\right)\right]\right\} + \frac{\delta x \delta t}{M_i^j}\left(Q_i^{j+\frac{1}{2}} - Q_i^{j-\frac{1}{2}}\right)$$

$$\tilde{v}_i^j = v_i^j + \frac{\delta x \delta t}{M_i^j}\left\{P_i^{j+\frac{1}{2}} - P_i^{j-\frac{1}{2}} + \frac{2}{\delta y}\left[\mu_i^{j+\frac{1}{2}}\left(v_i^{j+1} - v_i^j\right) - \mu_i^{j-\frac{1}{2}}\left(v_i^j - v_i^{j-1}\right)\right]\right\} + \frac{\delta y \delta t}{M_i^j}\left(Q_{i+\frac{1}{2}}^j - Q_{i-\frac{1}{2}}^j\right)$$

$$\tilde{I}_i^j = I_i^j + \frac{1}{2}\left[\left(u_i^j\right)^2 + \left(v_i^j\right)^2 - \left(\tilde{u}_i^j\right)^2\right] - \left(\tilde{v}_i^j\right)^2 + \frac{1}{2}\left(u_i^j + \tilde{u}_i^j\right) g\delta t + \frac{\delta y \delta t}{M_i^j}\left\{(Pu)_{i+\frac{1}{2}}^j - (Pu)_{i-\frac{1}{2}}^j + (Qv)_{i+\frac{1}{2}}^j - (Qv)_{i-\frac{1}{2}}^j\right.$$

(Equation continued)

$$+\frac{\mu_{i+\frac{1}{2}}^{j}}{\delta x}\left[B\left(r_{i+1}^{j}-r_{i}^{j}\right)+\left(u_{i+1}^{j}\right)^{2}-\left(u_{i}^{j}\right)^{2}\right]$$

$$-\frac{\mu_{i-\frac{1}{2}}^{j}}{\delta x}\left[B\left(r_{i}^{j}-r_{i-1}^{j}\right)+\left(u_{i}^{j}\right)^{2}-\left(u_{i-1}^{j}\right)^{2}\right]\Bigg\}$$

$$+\frac{\delta x\delta t}{M_{i}^{j}}\Bigg\{(Pv)_{i}^{j+\frac{1}{2}}-(Pv)_{i}^{j-\frac{1}{2}}+(Qu)_{i}^{j+\frac{1}{2}}-(Qu)_{i}^{j-\frac{1}{2}}$$

$$+\frac{\mu_{i}^{j+\frac{1}{2}}}{\delta y}\left[B\left(r_{i}^{j+1}-r_{i}^{j}\right)+\left(v_{i}^{j+1}\right)^{2}-\left(v_{i}^{j}\right)^{2}\right]$$

$$-\frac{\mu_{i}^{j-\frac{1}{2}}}{\delta y}\left[B\left(r_{i}^{j}-r_{i}^{j-1}\right)+\left(v_{i}^{j}\right)^{2}-\left(v_{i}^{j-1}\right)^{2}\right]\Bigg\}$$

Again, each quantity at a cell boundary is taken to be an appropriate average between the two adjacent cells. Perhaps the only feature of the finite-difference form which is not otherwise obvious is the manner in which the acceleration term is written in the energy equation:

$$\frac{1}{2}\left(u_{i}^{j}+\tilde{u}_{i}^{j}\right)g\delta t$$

rather than, say,

$$u_{i}^{j}\,g\delta t$$

Choice of the form shown is based on the requirement of rigorous energy conservation by the difference equations.

More details for a specific application of these equations are given in the discussion of results in Chapter VII.

D. Two-Dimensional Calculations in Cylindrical Coordinates

There are many problems which are characterized by independence of

the flow field from the angle about some fixed axis. Such cylindrical problems with axial symmetry can be treated by the PIC method with almost no modification of the procedure already outlined. Consider the problem of determining the motion of a single nonviscous, nonconducting fluid through an infinite periodic cylindrical pipe with rigid walls. In some plane through, and parallel to, the axis, one period of the flow field will be a rectangle, bounded at the bottom by the axis, at the top by the pipe, and at the left and right by the ends of the period. This region is divided into rectangular cells (actually toroids of revolution), and the fluid is again represented by particles (actually circles about the axis). In such problems it has been found convenient to assign different masses to the particles, each particle being given a fixed mass whose value is proportional to the original radius of the particle, so that the particle density is initially proportional to the true density.

The differential equations

$$\rho \frac{du}{dt} = -\frac{\partial p}{\partial r}$$

$$\rho \frac{dv}{dt} = -\frac{\partial p}{\partial z}$$

$$\rho \frac{d}{dt}\left[I + \frac{1}{2}\left(u^2 + v^2\right)\right] = -\frac{1}{r}\frac{\partial pur}{\partial r} - \frac{\partial pv}{\partial z}$$

become, for the Phase I calculations,

$$\tilde{u}_i^j = u_i^j + \frac{2\pi\, r_i^j\, \delta z \delta t}{M_i^j}\left(p_{i-\frac{1}{2}}^j - p_{i+\frac{1}{2}}^j\right)$$

$$\tilde{v}_i^j = v_i^j + \frac{2\pi\, r_i^j\, \delta r \delta t}{M_i^j}\left(p_i^{j-\frac{1}{2}} - p_i^{j+\frac{1}{2}}\right)$$

$$\tilde{\Gamma}_i^j = \Gamma_i^j + \frac{1}{2}\left[\left(u_i^j\right)^2 + \left(v_i^j\right)^2 - \left(\tilde{u}_i^j\right)^2 - \left(\tilde{v}_i^j\right)^2\right] - \frac{2\pi\ \delta z \delta t}{M_i^j}\left[(pur)_{i+\frac{1}{2}}^j - (pur)_{i-\frac{1}{2}}^j\right]$$

$$- \frac{2\pi\ r_i^j\ \delta r \delta t}{M_i^j}\left[(pv)_i^{j+\frac{1}{2}} - (pv)_i^{j-\frac{1}{2}}\right]$$

where u and v are the r- and z-direction velocity components, respectively, and i and j count cells in those respective directions. At the axis, u = 0, while a quadratic extrapolation of pressure, as discussed before, is appropriate. These difference equations are perfectly conservative. Moreover, they tend to preserve spherical symmetry. This fact is not in contradiction to the statements in Ref. 4 (p. 27) wherein the difference equations were written with differences between cell centers, rather than between cell boundaries. The present form of the equations also has the advantage of avoiding the peculiar boundary condition at the axis required in Ref. 4 [Eq. (52), p. 28].

The particle movement of Phase II proceeds by a velocity weighting proportional to areas, just as in Cartesian coordinates, rather than to volumes. A test of the latter procedure produced unsatisfactory results, especially near the axis. Again, if a particle does not cross a cell boundary, then there is no change to the cellwise quantities; if it does cross, then mass, "momentum," and energy are added and subtracted as before. (Here the radial-direction "momentum" is defined as the product of the mass and the radial velocity.)

Numerous calculations using the PIC method in cylindrical coordinates show that it is nearly as useful for such problems as for those in Cartesian coordinates, even when there may be large radial-direction motions of the fluid. Results of one series of cylindrical problems are discussed in Chapter VI.

E. Limitations of the Method

The PIC method has been found useful in solving a wide variety of problems concerning the dynamics of compressible fluids. Very little analytical work has been accomplished in the direction of proving the validity of results, so that considerable experimentation has been necessary. The range of applicability is discussed in this report and elsewhere; it is also appropriate again to emphasize the limitations.

The principal limitation of the PIC method arises from the requirement that the fluid speed relative to the computational mesh must not be small compared with the sound speed. An exception is allowed in a uniform region, where the fluid speed may be zero. Thus it is not possible to apply the method to problems in incompressible-fluid flow. There are two related reasons for this restriction. First, interactions within the fluid are propagated only from cell to cell, whereas in an incompressible fluid, the changes in configuration at a point depend upon conditions at that instant throughout the fluid. Second, as the fluid speed decreases, the "effective viscosity" due to the dissipative procedure used in cell crossings (Ref. 4, p. 16) decreases to zero. The difference equations, in this limit, can be shown to be unconditionally unstable. Thus, in a region of "perturbed stagnation," fluctuations of the field variables grow until the velocities are large enough to produce sufficient dissipation. A further discussion of this matter is given in Ref. 6, page 10. This second difficulty can be relieved somewhat by the incorporation of artificial dissipative terms into the difference equations. Usually such terms also have somewhat undesirable results, such as the increased smearing of discontinuities. A discussion of these extra terms is in preparation by Longley.[8]

Another significant limitation of the PIC method results from the inability of the fixed mesh of cells to resolve features of the flow field which

are small in size compared to the over-all region to be studied. In some cases the limitation can be overcome by the creation and destruction of cells, so that computational mesh is present only where needed. It would also be possible to have fine zones at some localities and coarse zones at others, but such a procedure has not yet been tried.

CHAPTER II

SHOCK-WAVE REFRACTION AT A GASEOUS INTERFACE

A. Introduction

In a recent paper, Jahn[9] presented the results of a set of experiments designed to study the regular and irregular refraction patterns arising from the interaction of a shock with an oblique interface between two gases. Results of his regular-refraction experiments agree closely with the theoretical results of Polachek and Seeger.[10] The experiments also revealed several types of irregular refraction process, for which no comparison theory existed. Jahn discussed these patterns and showed that they could be explained qualitatively by application of simple gas-dynamic principles. His discussions, in amplified form, are also given in a series of Princeton University reports.[11]

The experimental set-up consisted, ideally, of a two-dimensional channel in which there was, initially, an oblique, essentially-massless diaphragm separating two gases in equilibrium. A plane, steady shock was allowed to approach through one of the gases and interact with the interface, and the result was photographed during the interaction. As such, the experiments differed from the theoretical model assumed by Polachek and Seeger, and by Taub[12] in his similar calculations. In the model, the interface was of infinite extent, and no effects from the corner were considered. In the experimental work, Jahn was able to separate the corner effects from those

of the pure refraction by suitable adjustment of the angle of the channel wall just beyond its intersection with the corner. These corner effects cannot be completely eliminated, however, and any complete theoretical description of the processes must include them.

Because no initial assumptions concerning the nature of the interaction are required in PIC-method calculations, it was expected that both regular and irregular refraction processes, together with corner effects, could be computed. Some representative calculations were carried out, and the results confirmed the expectations and exhibited well certain properties of the method.

In the calculations the gases were considered to be nonviscous, nonconducting, and polytropic. They were confined between rigid parallel walls in a two-dimensional channel, with shock input on the left and a continuative boundary on the right. Each was initially homogeneous and the two were at the same pressure. The section of channel studied was divided into 1200 square computational cells, having a maximum average of four particles per cell. The interface between gases was inclined at 45° in all calculations. This was the easiest angle to represent in the mesh of square cells; the angle could be changed if rectangular cells were allowed, or if the particle placements were altered. With the angle chosen, however, all features of interest for this study were revealed.

The best representation of an input shock is obtained if the average number of particles per cell behind it is an integer. Therefore, in each case the density ratio across the incoming shock was required to be four to two.

The results of the calculations are presented mainly in the form of illustrations of the flow configuration at suitable times during the interactions. Each picture was formed by plotting the positions of all the mass

points in the system and superimposing an interpretation of the main features by lines representing shocks, slip planes, and rarefaction fronts. These positions were, in every case, determined by observation of deflections of the mass-point lines. Where the signals were weak, the results of this procedure were not always in good agreement with known results; the details are discussed in the individual cases, and it is pointed out that there are usually other satisfactory means of locating the weak-signal positions. Certain peculiarities of the mass-point plots are discussed below in connection with Fig. II-1.

Numerous other results were also obtained from the computations. These included internal and kinetic energies of each gas and other functionals of motion such as the vertical and horizontal momenta. Because these were considered to be of less interest here, they are discussed only briefly in a few cases. Among the least reliable results from the calculations are such quantities as local, instantaneous densities. These and other local features which depend upon the number of mass points per cell may fluctuate rather strongly about their true values. It is an essential feature of the computing method, however, that the gross functionals of motion (those which extend over numerous cells or depend upon time averaging) are well reproduced in spite of these local fluctuations.

In our computations, the gases have been considered to be nonviscous, non-heat-conducting, and polytropic. Effects from the computing-method approximations, however, can be interpreted as imparting certain other characteristics to the gases. Principal among these is an effective "viscosity" which allows for the calculation of shocks, but which also results in a shear adhesion. This is mathematically similar to true viscosity but differs, for example, in being anisotropic in a manner dependent upon the orientation of the coordinate system. The effects are clearly visible in the results reported

in this chapter, but are unimportant in their effect on most features of interest.

We have used the notation of Jahn, according to which the initial shock I of strength ξ (ξ = ratio of pressure ahead to pressure behind) is incident from the left on the interface O. In the resulting configuration, there is a reflected shock RS or reflected rarefaction RR, a deflected interface D, and a transmitted shock T. In Table II-1 are tabulated the essential features of the problems.

Table II-1

LIST OF COMPUTATIONS

Problem Number	Gas Combination	ρ_R/ρ_L	γ_L	γ_R	ξ
1	Air/CO_2	1.529	1.405	1.304	0.362
2	Air/CH_4	0.554	1.405	1.310	0.362
3	Air/Neon	0.696	1.405	1.667	0.362
4	Air/Polytropic Gas	0.237	1.405	1.667	0.362
5	Air/He	0.138	1.405	1.667	0.362

B. Regular Refraction with Corner Effects

With the restrictions previously mentioned, it was not possible to calculate for any situation corresponding exactly to an experiment by Jahn. Instead, as a check on our results we calculated points on two of the curves of Polachek and Seeger, choosing curves on which several points had been verified by Jahn's results.

The interaction configuration for problem 1 is shown in Fig. II-1.

This regular refraction pattern consists of transmitted and reflected shocks, and a smoothly deflected interface. Also visible is the corner signal (a rarefaction wave) which, in its propagation along the interface through the air, induced a more slowly traveling rarefaction signal in the CO_2. Interaction of the oblique transmitted shock with the channel wall resulted in a Mach reflection pattern. The effects of various weaker disturbances can be seen in the pattern of mass points in the lower part of the air.

There are certain features of the mass-point plot and interpretation which also apply to the other illustrations. First, it is apparent that there is a vertical discontinuity in the pattern of the plus points. Those to the right of the discontinuity were present in the calculation region at initial time, those to the left entered subsequently, and the manner of their introduction was not such as to produce the same pattern as resulted from compressing the gas already present. The deflections of the vertical or diagonal mass-point lines are more significant in the determination of boundaries in the flow pattern than are those of the horizontal. Indeed, near the deflected interface, at which there should be slippage, the effective "viscosity" arising from the computing method caused rather strong deflections of the horizontal mass-point lines.

The most clearly discernible features are the interface position and the positions of the initial and transmitted shocks. Location of the corner and reflected signals is usually difficult and requires the use of a straightedge placed along the mass-point lines. In problem 1, the reflected signal, a shock, was extremely weak. As a result, its location as determined by the mass-point-line deflections is not as high as it should be; the angular discrepancy is about 7°. Reference to the detailed cellwise listings of the calculation, however, shows that a signal had actually penetrated higher than is shown in Fig. II-1, and good agreement with the correct result can be

obtained by drawing a line through the group of uppermost cells, each of which shows any change in temperature from that in the cells above it. The positions of the interface and of the transmitted shock, however, are in good agreement with the correct positions, differing in angular deflection by approximately 2° and 0° respectively. The position of the corner signal is likewise consistent with the expected position as determined by the sound speed in the air behind the reflected shock.

The results for problem 2 are shown in Fig. II-2. In this case, the computed angular deflection of the interface was too great by about 3°, while that of the transmitted shock was too small by about 2°. Again, the reflected signal (a rarefaction) was too low, as measured by mass-point-line deflections, with an angular discrepancy of about 7°. The primary signals from the corner are more complicated in this calculation. They include a weak signal which propagated rapidly through the methane and a stronger signal whose propagation rate along the interface through the air was nearly the same as that observed in problem 1. The strength of this second signal (a shock) was great enough so that a following rarefaction was produced; this, in turn, induced a rarefaction in the methane. In the lower part of the region, there are numerous signals whose effects on the interface are shown by the flexures thereof. A plane of considerable slippage has been drawn in.

In both problems 1 and 2, the accuracy of the calculations is consistent with the resolution to be expected from this size of finite-difference cells. The most apparent discrepancies are in the reflected-signal positions, when they are weak; but, in these and other calculations, such weak-signal locations can be determined by reference to detailed listings of cellwise temperatures.

C. Irregular Refraction

We have investigated, in particular, the irregular refraction pattern

arising when the right-hand gas has a higher sound speed than that of the left-hand gas. We were especially interested in studying cases similar to those in which the experiments showed the deflected interface to be unstable [Ref. 9, Plate 6, Fig. 14(c) and Plate 12, Fig. 18].

The irregular refraction pattern and the unstable interface were both observed in the calculation of refraction from air to helium. To study the development of these, we performed a sequence of calculations. The first one—a regular refraction from air to neon—is shown in Fig. II-3. The configuration is particularly simple; the corner signals were weak and the deflected interface is nearly straight. The reflected shock was extremely weak and is not shown. In the lower part of the air there are indications of a slip plane and a rarefaction. These became progressively more evident in the subsequent two calculational results.

In the next calculation, the density of the right-hand gas was reduced to a value intermediate between those of neon and helium, and the temperature (hence also the sound speed) was increased for initial equilibrium. As a result, the transmitted-shock speed along the interface was greater than that of the input shock, and detachment occurred. The configuration is shown in Fig. II-4. The reflected shock is now evident, as is its strong modification by the following rarefaction. The slip plane and rarefaction in the lower air were much more strongly developed than in problem 3. The deflected interface showed some instability; adjacent to it, the right-hand gas was turbulent, while the air remained fairly stable.

The air-to-helium refraction pattern, presented in Fig. II-5, shows a strong development of the irregularity as well as a great instability of the interface and of the shocked helium. The irregularly reflected shock interacted with the rarefaction, and the resulting disturbance was somewhat weakened. The lower slip plane and rarefaction in the air were even more

strongly developed than before. The result of continuing the calculation to a later time is shown in Fig. II-6.

It is not thought that the structure of the deflected interface is correctly represented in detail. Just as in an experiment, the exact nature of the structure depends on the form of the initial interface irregularities, as well as on the nature of interactions with the complicated, small-scale structure of shocks and rarefactions. In the calculation, the initial irregularities of the interface correlate with the nature of the finite-difference mesh, and many of the small-scale structures are not resolved by that mesh. Nevertheless, it seems significant that the computed refractions are stable in many cases and become unstable in circumstances under which the experimental patterns are also unstable.

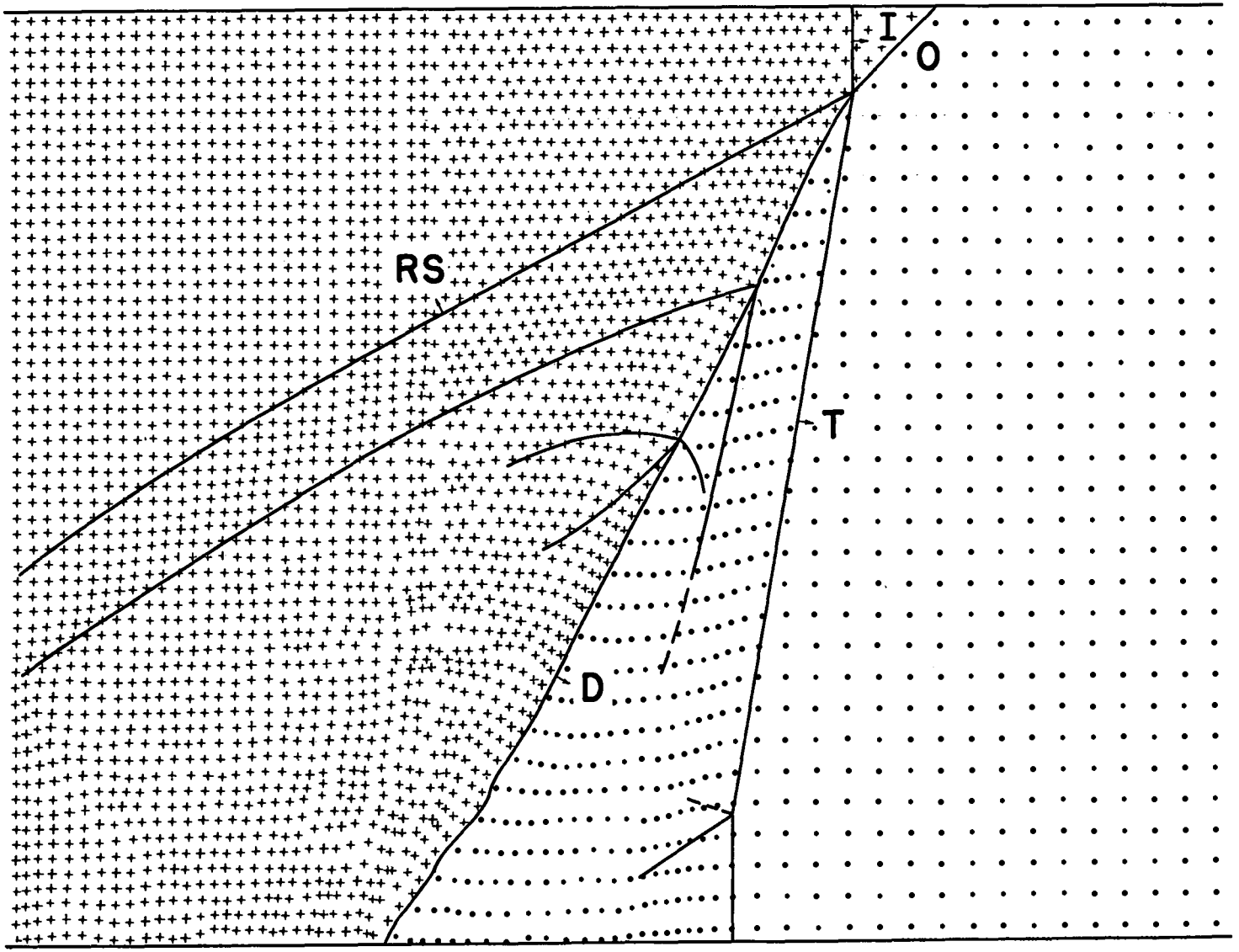

Fig. II-1 Interaction configuration for problem 1.

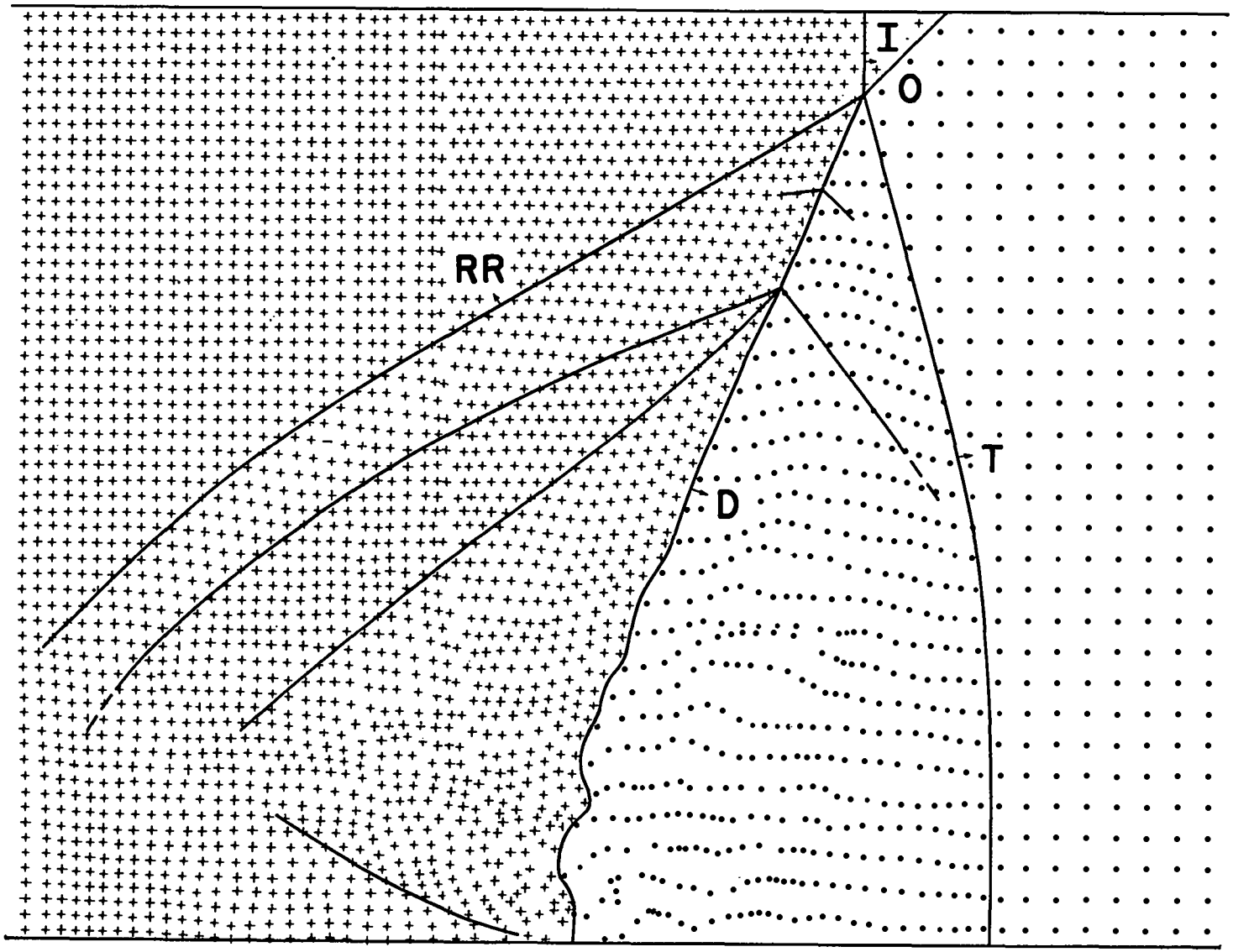

Fig. II-2 Interaction configuration for problem 2.

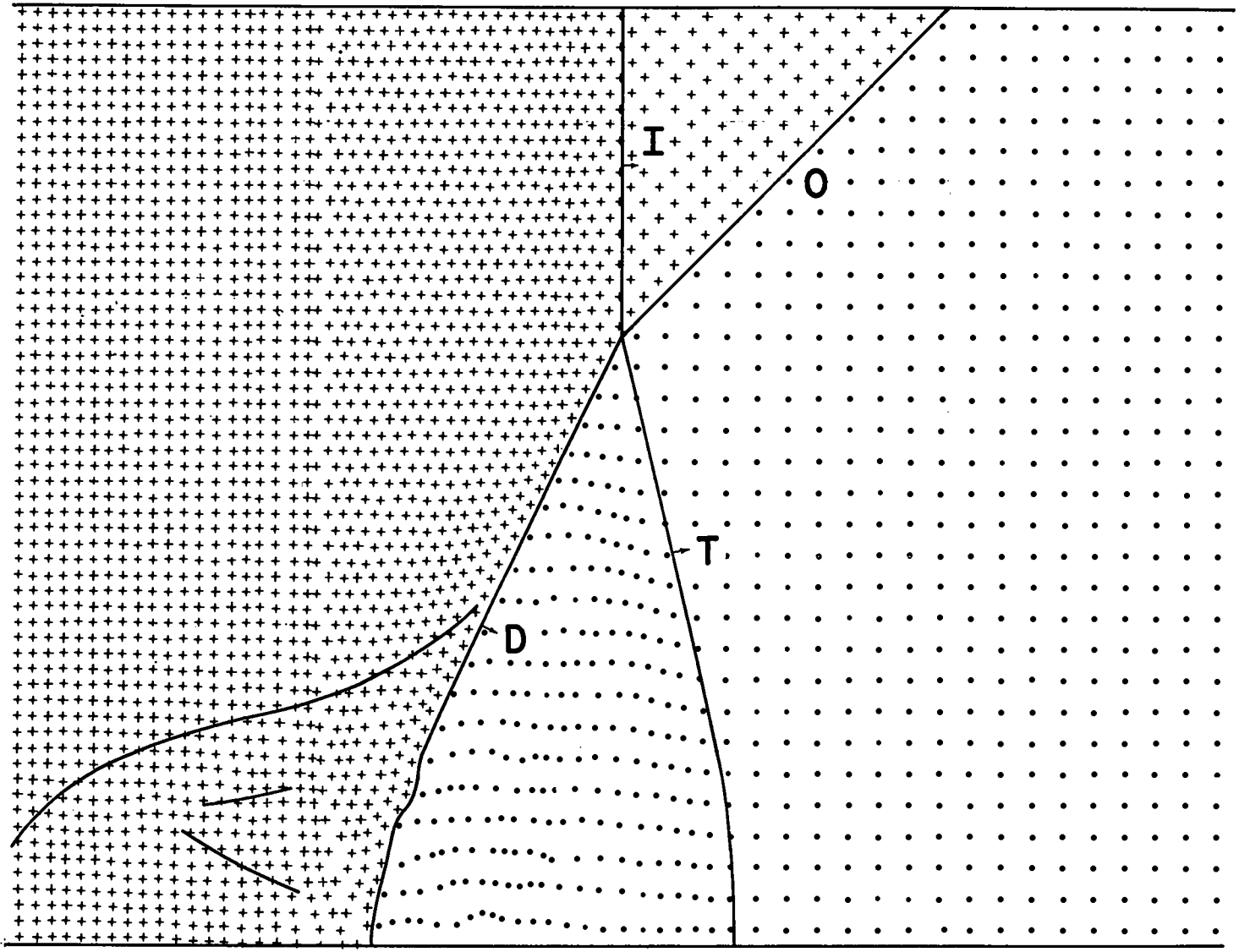

Fig. II-3 Interaction configuration for problem 3.

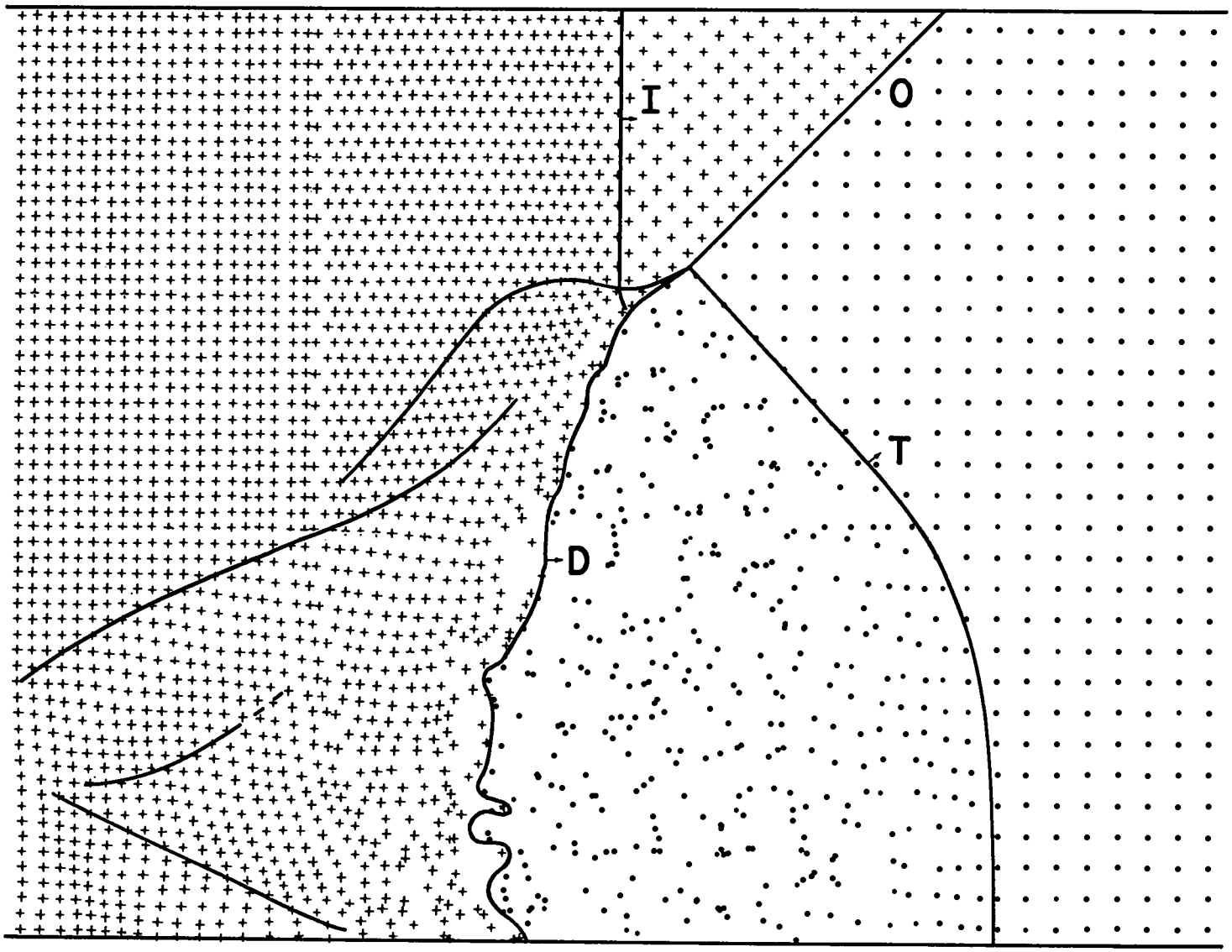

Fig. II-4 Interaction configuration for problem 4.

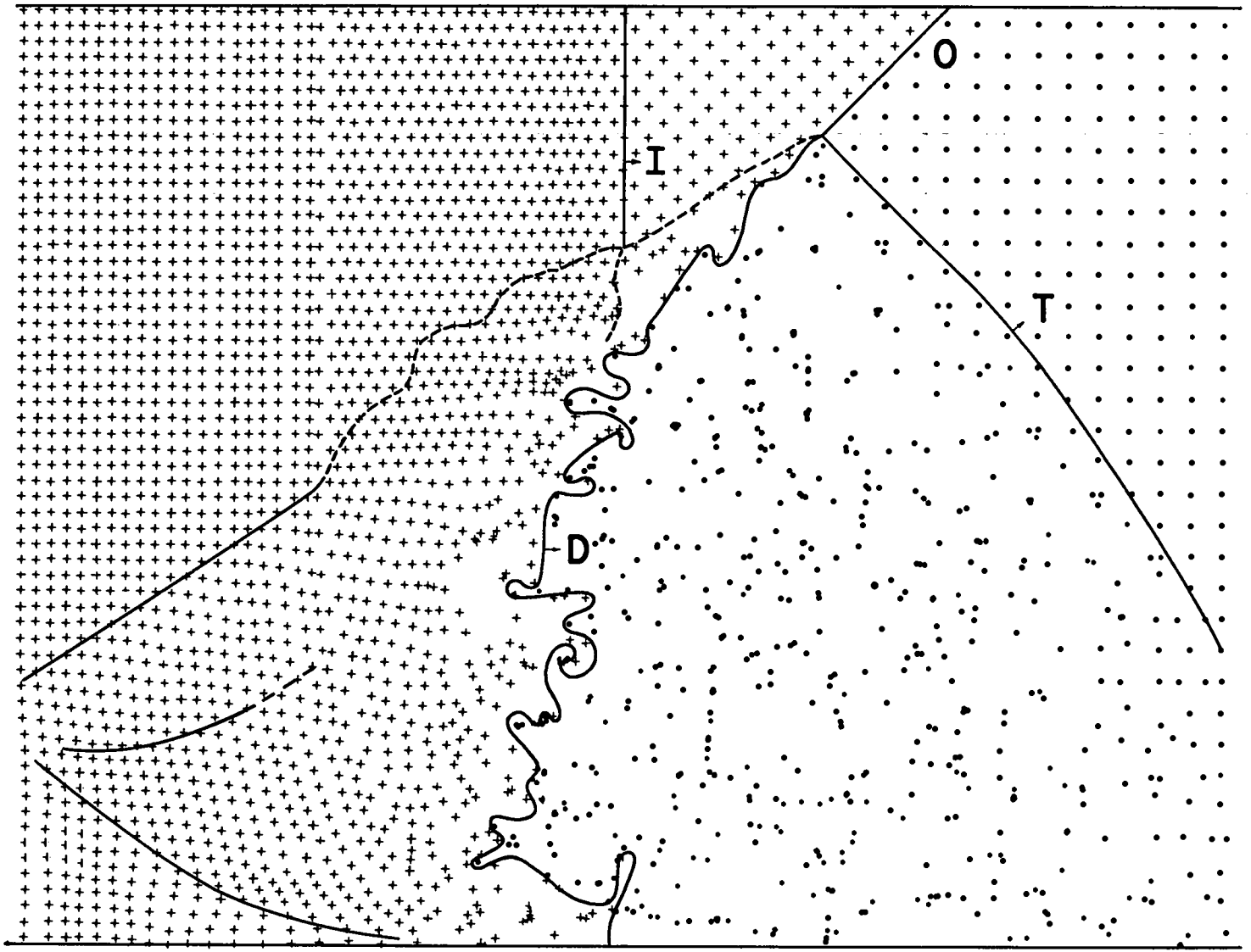

Fig. II-5 Interaction configuration for problem 5.

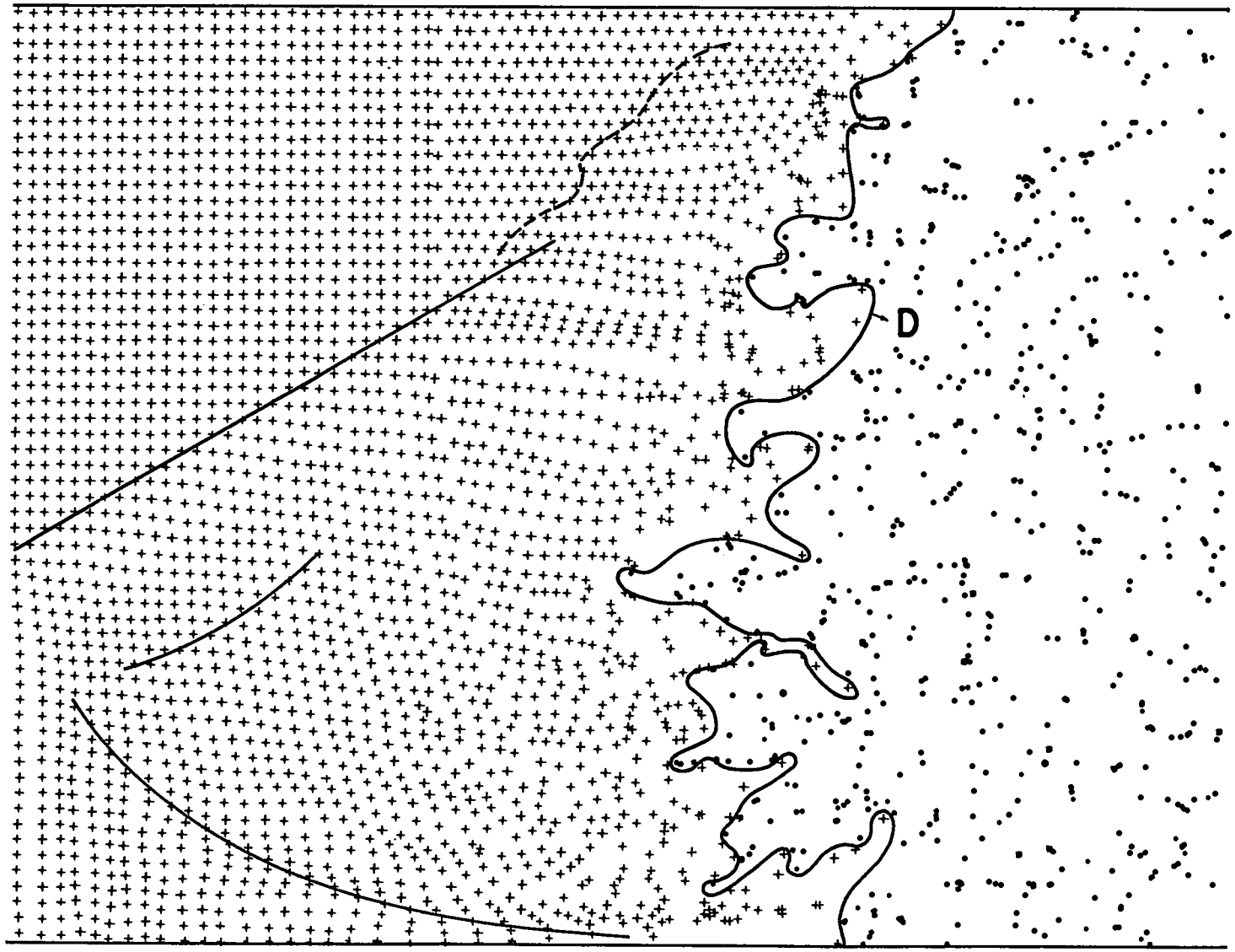

Fig. II-6 Late-time interaction configuration for problem 5.

CHAPTER III

SHOCK PASSAGE THROUGH A DISCONTINUOUSLY ENLARGED CHANNEL

A. Introduction

Considerable attention has been paid to the problem of determining theoretically the changes in a shock as it passes through a channel of variable cross section. The problems for weak shocks or gradual area changes have been treated by numerous authors from several points of view. Only a moderate amount has been written, however, about the more difficult problems associated with the passage of a strong shock through a channel with rapidly varying cross section. Whitham[13] has devised an approximation method which should be useful in many cases. A different approach has been used successfully by Laporte[14] for constricted channels. It does not seem likely, nevertheless, that any analytical treatment which might be developed in the near future will be capable of describing the entire flow field in these complicated cases, but that solutions for particular situations will have to be obtained by use of special numerical techniques.

In this chapter, we describe the application of the PIC method to the special problem of determining the two-dimensional flow of a strong shock through a discontinuously enlarged channel formed by two rigid planes which are parallel except at the discontinuity. There, one of the planes has a double right-angle bend, doubling the channel width. This is one element,

in simplified form, of some of the problems which arise in studies of shock damage to building interiors and in questions concerning establishment of flow patterns in a shock tube. In this situation, development of the flow field with time can be divided into two phases. In the first, the shock, which approached from the narrow side, diffracts about the corner. Behind it, there is established a complicated structure which includes an expansion fan, together with several shocks and slip lines. The entire structure retains geometric similarity as it expands linearly with time. In the second phase, the shock interacts with the wall of the enlarged channel, is further modified, and the flow near the corner eventually becomes nearly steady.

The features of both phases are discussed in some detail in this chapter. In addition, comparisons with experiments are presented for the first phase of development. For the experimental results, we are grateful to Dr. Russell E. Duff who generously made available unpublished photographs of the results of experiments performed with nitrogen at the Shock Tube Laboratory, University of Michigan, in 1950.

B. The Computations

Two different gases were studied, nitrogen and helium. They were considered to be polytropic, nonviscous, and non-heat-conducting, with specific heat ratios $\gamma = 1.404$ and $\gamma = 1.667$, respectively.

In each of the computations, the Mach number behind the initial shock was greater than unity so that no changes in flow occurred in the narrow section of channel, in this instance to the left. Thus, the region of computation was chosen to cover a rectangular section of channel just to the right of the discontinuity. In the three problems with nitrogen, the region was shorter along the channel length in order that the best possible resolution could be obtained near the corner. In the problem with helium, the

region was longer along the channel length in order that down-channel effects could be studied.

At the upper half of the left boundary, the input represented the steady flow behind the initial shock which, at time t = 0, was at the discontinuity. At the right, the boundary condition was continuative. The channel walls were treated as rigid and reflective with perfect slippage. At initial time, the gas in the computation region was homogeneous and at rest, represented by two mass points per cell. Units were scaled so that a cell length was unity, and the undisturbed gas was at unit density. In the undisturbed nitrogen, the sound speed was unity; however, the shock in helium was of infinite strength, and in this case the material speed behind it was initially unity. The units of time were accordingly chosen.

C. Development of the Flow Patterns in Nitrogen

The larger section of channel was 40 units high, and the region of study extended 30 units to the right of the discontinuity. Calculations were performed for three different strengths of the initial shock.

The configuration of mass points at time t = 12.593 is shown in Fig. III-1 for the case in which the Mach number behind the shock was M = 1.008. The solid lines represent the shock and rarefaction fronts as deduced from the deflections of the mass-point lines. The long-dashed curves were taken from a photograph by Duff. The short-dashed curve is theoretical Prandtl-Meyer streamline. The mass points plotted by dots are those which were in the region at t = 0; those plotted by pluses entered subsequently. (The individual mass of a plus point was not the same as that of a dot point, so that the apparent density discontinuity between them is not real.)

A similar configuration is shown in Fig. III-2 for time t = 6.329. In

this case, the Mach number for flow behind the shock was M = 1.588.

In both cases, the shape of the diffracted shock is represented to within the expected resolution of the computations, while the rarefaction front, as determined by deflection of the mass-point lines, falls somewhat below the experimentally observed position. The discrepancy is not surprising. Where the upward-traveling signal was weakest, the deflections of the mass points were so small as to be undetectable in the plot. Reference to detailed cellwise listings of results from the computations shows, however, that a signal had indeed penetrated higher than the position shown by the particle-line deflections, and approximate agreement with the experimentally observed line can be obtained by an appropriate interpretation of the listings. The situation is the same as encountered with the reflected signals in Chapter II.

It is not expected that the Prandtl-Meyer streamline should lie along a mass-point line in the early development of the flow. The first tendency of the mass-point lines is to curve downward; for weak shocks, this tendency results in the formation of the well-known spiral vortex. As the flow continues, however, the mass-point lines should approach the streamlines. This expectation was closely realized in the two computations which were extended to late times. In them (one case is shown in Fig. III-6), the hand-computed Prandtl-Meyer streamlines lie very close to the mass-point lines up to the point where the flow is perturbed by reflection from the channel bottom.

The configuration for M = 1.296 is shown in a slightly different way in Fig. III-3. The time is t = 10.063. The fine lines connect mass-point lines which formed a square grid in the initially unshocked gas, as shown in the lower right-hand corner. The computed shock and rarefaction fronts were again determined by the deflection positions of these lines. The experimental positions are shown as dashed lines; also included in this figure

are the details of additional flow structure observed on the photograph (Fig. III-4) near the diffracting corner. On the photograph the two lines diverging from the corner represent the end of the expansion fan and the slip stream. The former is truncated by a shock. These structures are suggested by the computations, but the lack of resolution with this coarse cell size precluded reproduction of the details. The structure just below the corner is not clearly correlated with any feature of the computations. The experimentally observed curved line behind the shock, and approximately parallel to it, is represented in the computation by a thin region of strong slip and of compression gradient, as shown by the mass-point-line positions.

Structures similar to these are also present in photographs (not shown) for the other two Mach numbers, corresponding to Figs. III-1 and III-2, but likewise in these cases the computation did not well reproduce the details.

Figures III-1 and III-2 show a region of instability in the flow field just below the corner. The boundary between incoming gas and that which was initially in the computation region folds back and forth in a manner suggesting Helmholtz instability. Positions of this line at two different times are shown in Fig. III-5 for the computation with M = 1.296. This computation was continued to considerably later times. Shortly after t = 20.127, the regularly folded structure of the interface was no longer recognizable, and by t = 35 the region of mixing had reached the right side of the computation region.

By t = 51.178, considerable of the original gas was still trapped in the lower left corner. The configuration of mass points at this late time is shown in Fig. III-6. The position of the rarefaction front where it is weak is not well indicated by the mass-point-line deflections. Some effect of the reflection of the rarefaction from the upper channel wall is suggested by the appearance of the upper right corner of the region.

D. Functionals of Motion

Until a signal from the corner has reached the top or bottom of the channel, all quantities in the disturbance region should be functions of only the ratios of the position coordinates to the time, and not otherwise depend on time. As a consequence, such functionals as vertical momentum and excess kinetic energy (over input) should increase exactly quadratically with time. The first of these can be computed by hand, and the result serves as a check of the machine computation. The result for the case with $M = 1.296$ is shown in Fig. III-7. In the early stages, the computed-momentum curve is indistinguishable from the theoretical one, whose extension is the dashed line. At $t = 10.7$, the shock arrived at the right-hand end of the computation region and, shortly thereafter, it began to interact with the channel bottom. Thus, the computed-momentum curve departs from the theoretical one. Much later, the flow in the computation region was in nearly a steady state, at which time the vertical momentum was nearly constant.

In Fig. III-7 there also is shown the average specific internal energy of a 5×5 square at the lower left of the computation region. The effect of shock arrival just before $t = 12$ is clearly visible.

In each of the three problems, the total kinetic energy in the computation region rose almost precisely at the rate of the flux across the input boundary during the first phase of development, indicating that kinetic and internal energy were nearly conserved separately during this time. Thus, the increase in kinetic energy which the gas received in the expansion fan must have been matched closely by the decrease as the gas decelerated at the back of the curved shock.

E. Infinite Shock in Helium

A calculation similar to those described above was performed for an infinite shock in helium. In this problem, the enlarged section of channel was 30 units high, and the region of computation extended 40 units along the channel. The flow pattern for time t = 30 is shown in Fig. III-8 and that for time t = 70 in Fig. III-9. With the elongated calculation region, it was possible to see the reflected shock from the turbulent region along the channel wall. Local mean-velocity vectors, whose magnitudes can be compared with the input-velocity vector, show a divided flow in the turbulent region. In the lower left corner, the fluid was slowly and irregularly rotating; the upper part interacted irregularly with the main stream, and occasionally small amounts were rapidly carried away, some being fed back into the vortex and the rest being carried downstream.

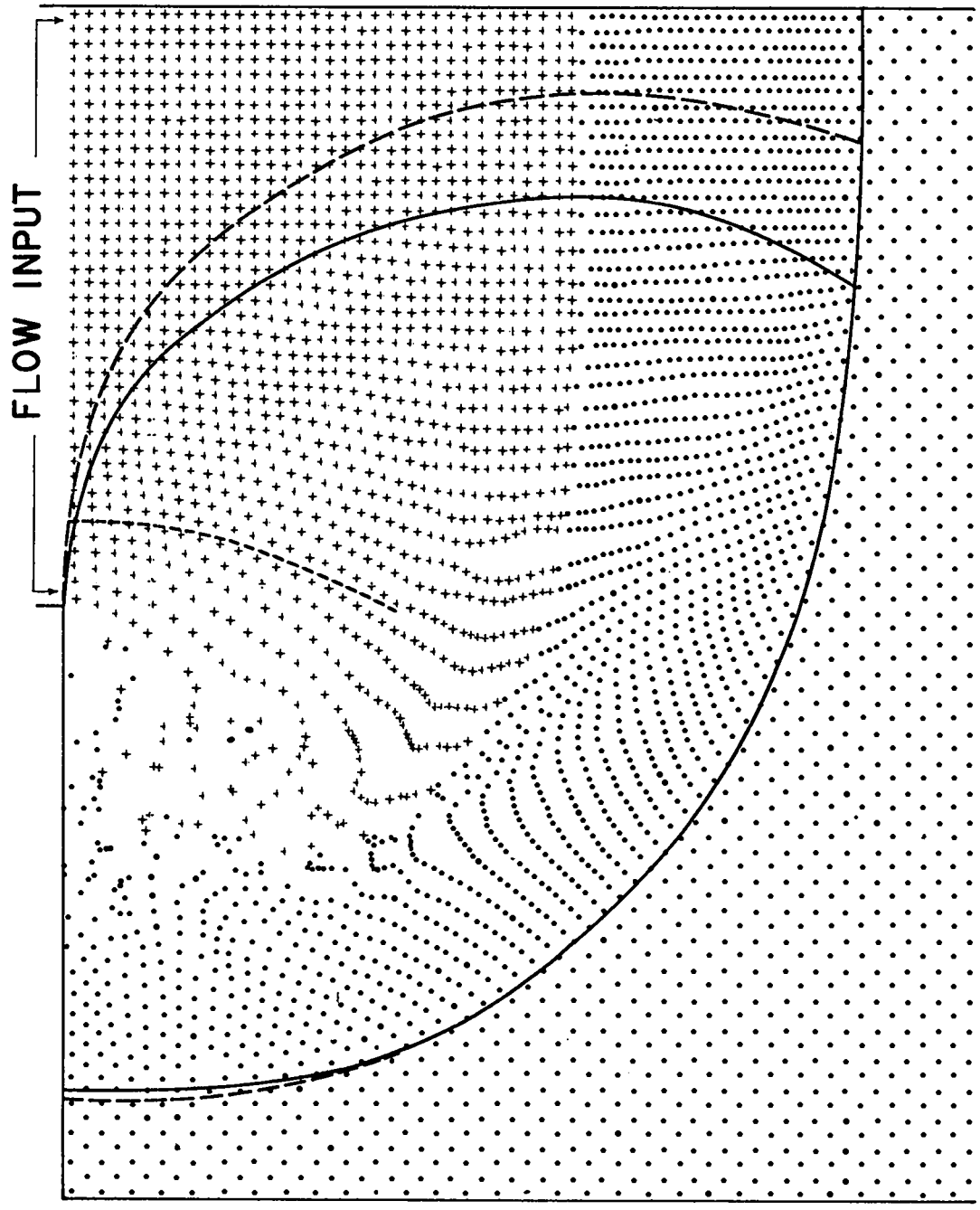

Fig. III-1 Configuration of mass points at time t = 12.593 for the calculation for nitrogen with M = 1.008. Solid and long-dashed lines represent, respectively, the computed and observed positions of shock and rarefaction fronts. Short-dashed line is a theoretical Prandtl-Meyer streamline.

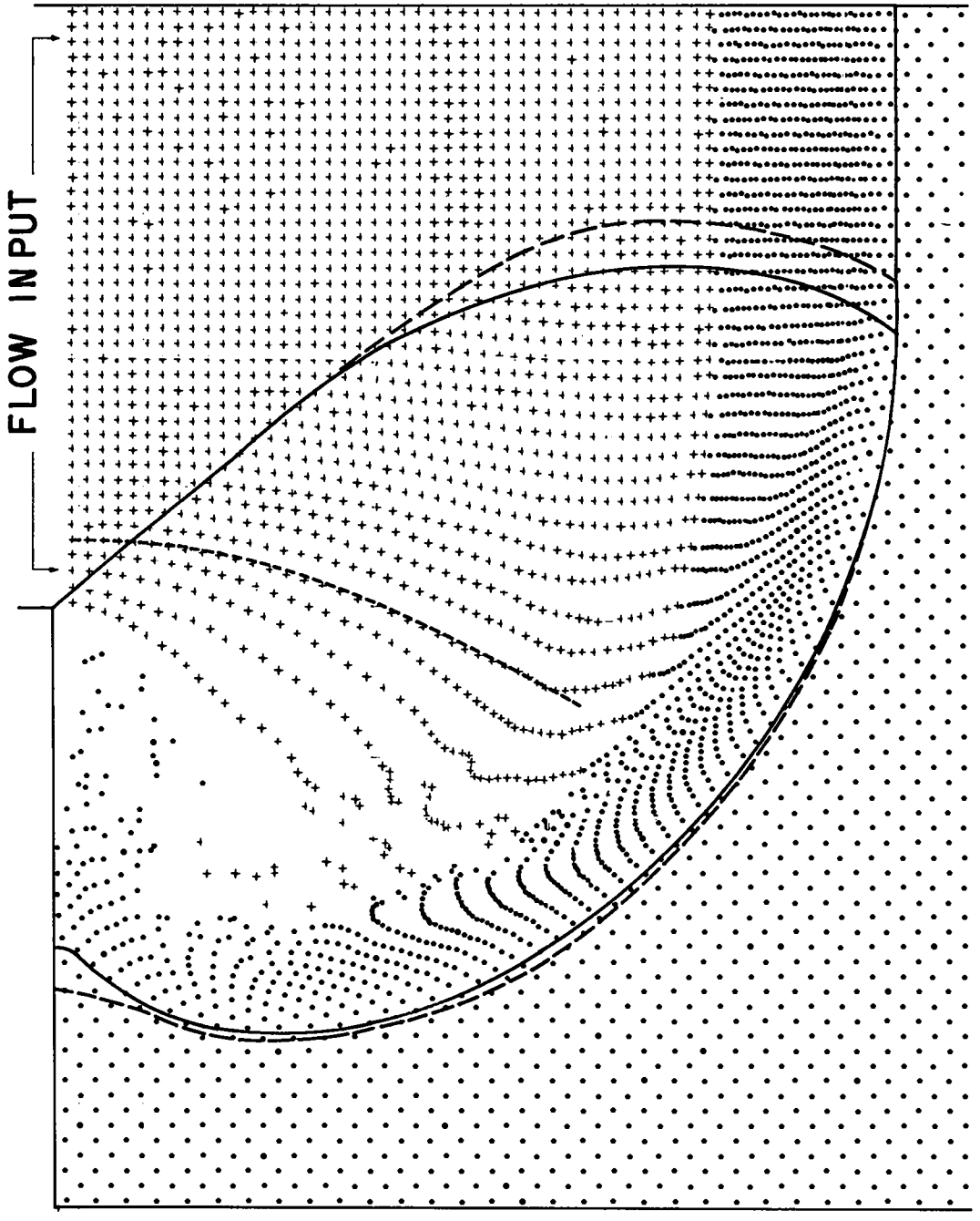

Fig. III-2 Configuration of mass points at time t = 6.329 for the calculation for nitrogen with M = 1.588. Solid and long-dashed lines represent, respectively, the computed and observed positions of shock and rarefaction fronts. Short-dashed line is a theoretical Prandtl-Meyer streamline.

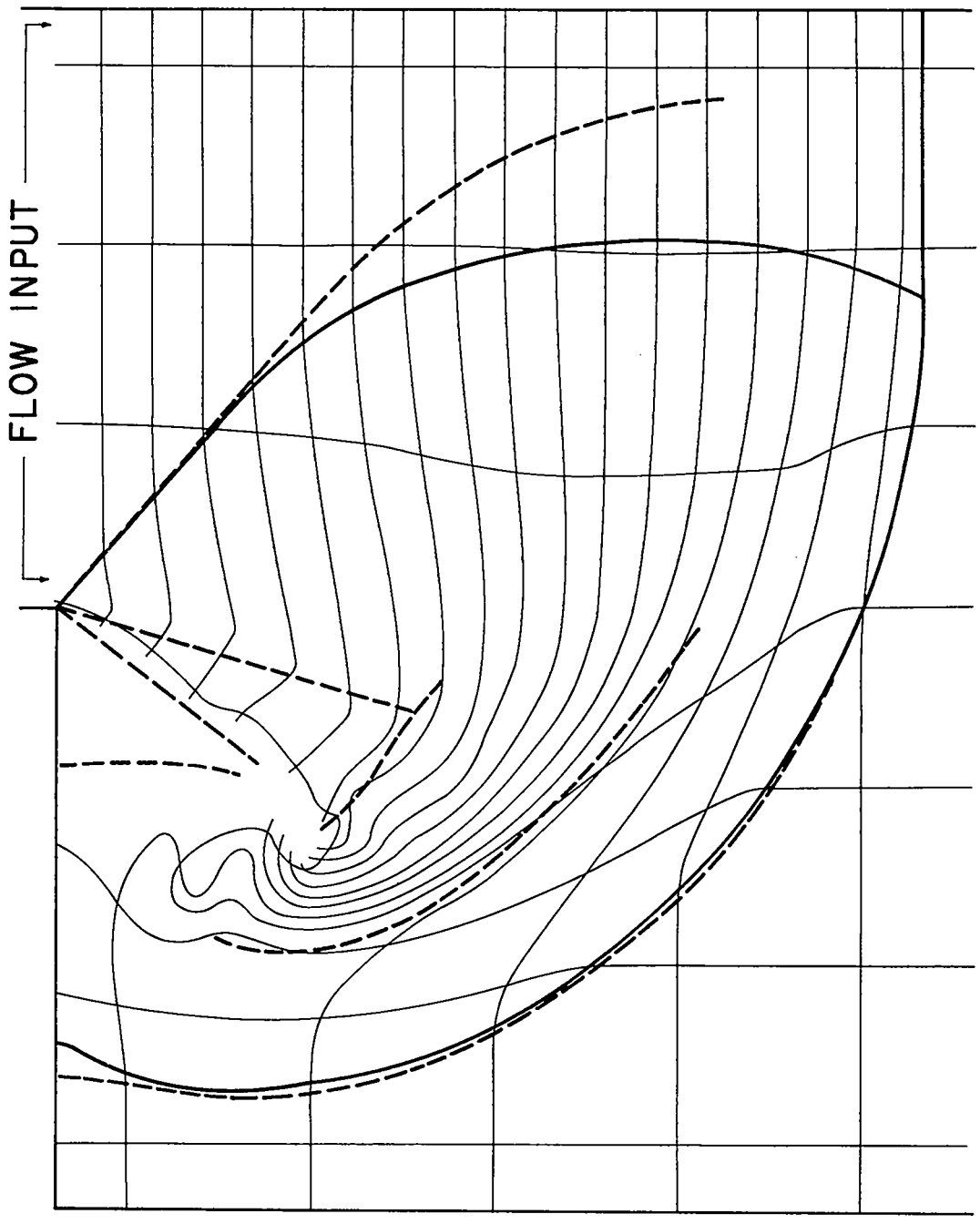

Fig. III-3 Configuration of some of the mass-point lines at time t = 10.063 for the calculation for nitrogen with M = 1.296. Heavy solid lines represent shock and rarefaction front positions. Dashed lines represent these, together with additional observed structure, as derived from a photograph, Fig. III-4.

Fig. III-4 Schlieren photograph by Duff of the flow field structure in nitrogen with M = 1.296.

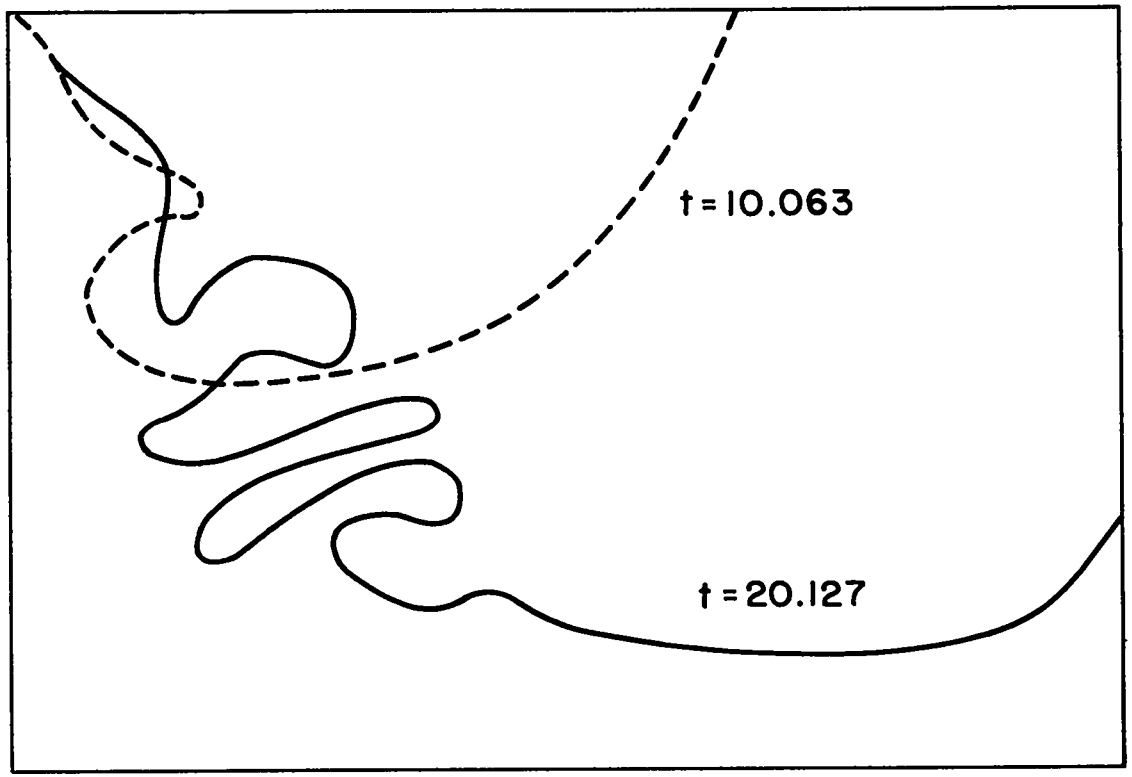

Fig. III-5 Boundary between incoming gas and that which was in the region at t = 0 for the calculation for nitrogen with M = 1.296. Only the lower half of the computation region is shown.

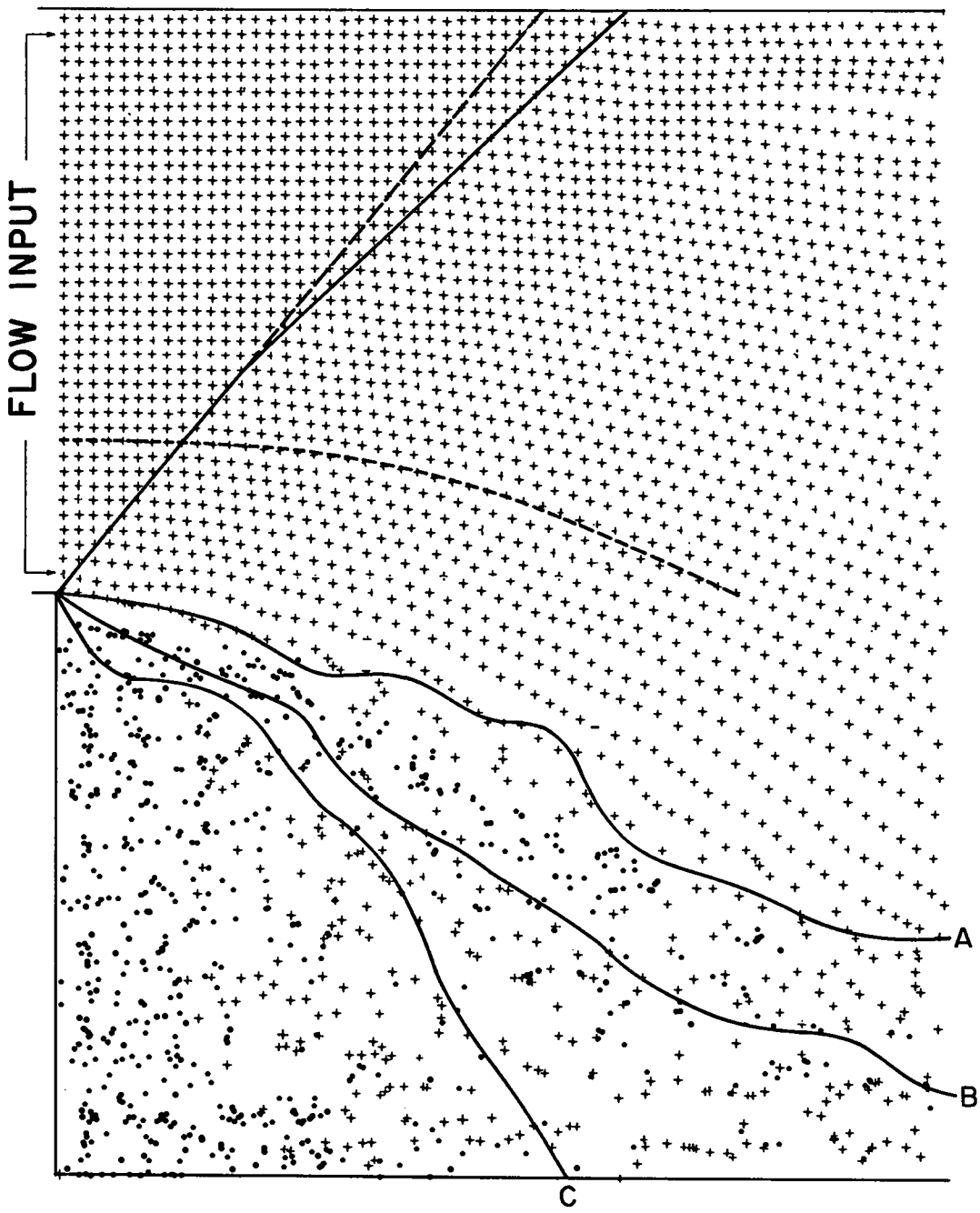

Fig. III-6 Configuration of mass points at t = 51.178 for the calculation for nitrogen with M = 1.296. From lines A to B, the gas speed drops by a factor of two. To the left of line C, the vertical gas motion is predominantly upward. Computed and theoretical Mach lines are shown as solid and long-dashed, respectively. Short-dashed line is a theoretical Prandtl-Meyer streamline.

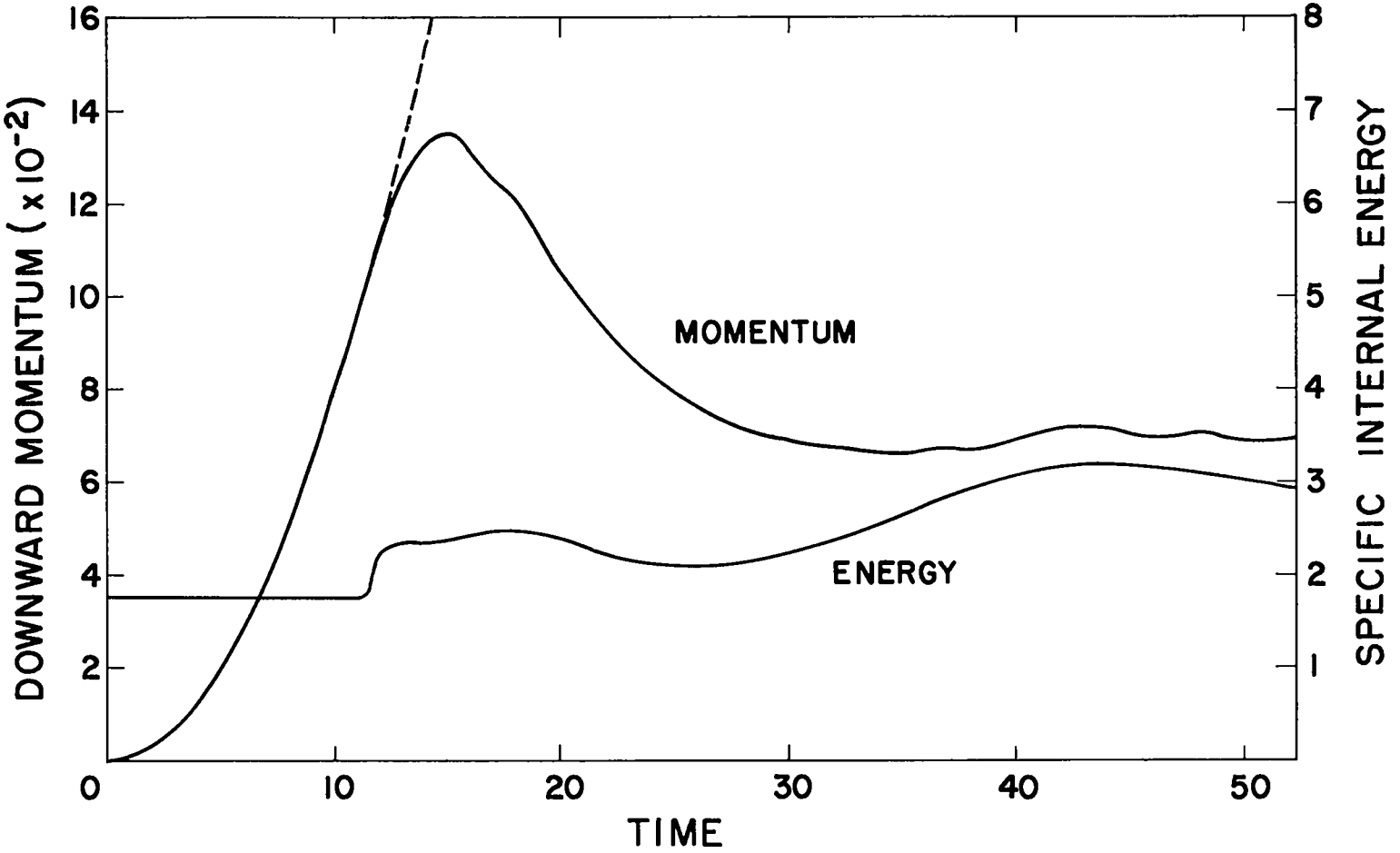

Fig. III-7 Downward momentum of the nitrogen in the computation region for the problem with M = 1.296. Dashed spur is extension of theoretical curve for early times. Also shown is the average specific internal energy in a 5 × 5 square at the lower left of the computation region.

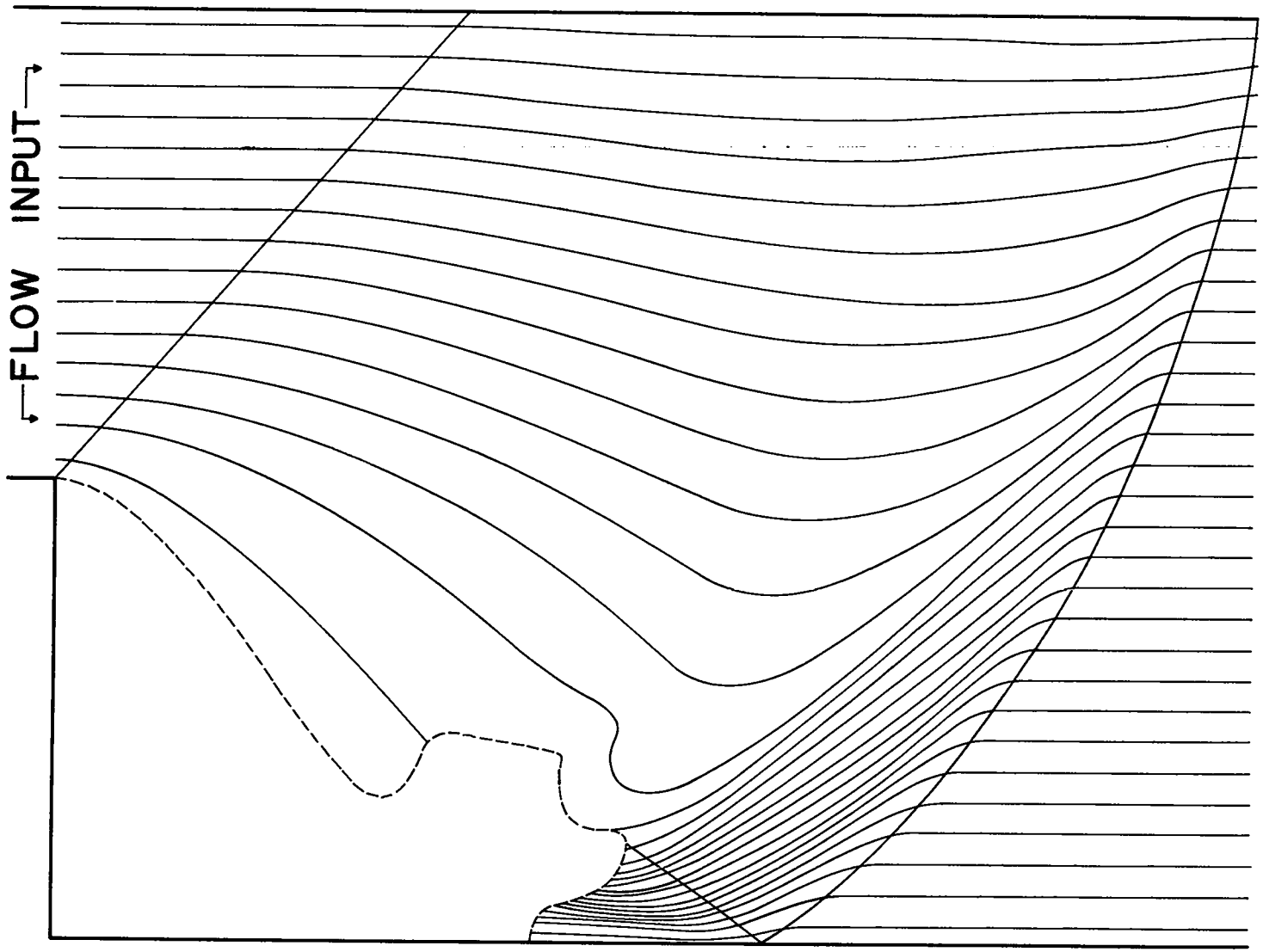

Fig. III-8 Configuration of the flow pattern at t = 30 for the calculation for helium, showing mass-point lines, shock front, Mach line from corner, and boundary of turbulent region.

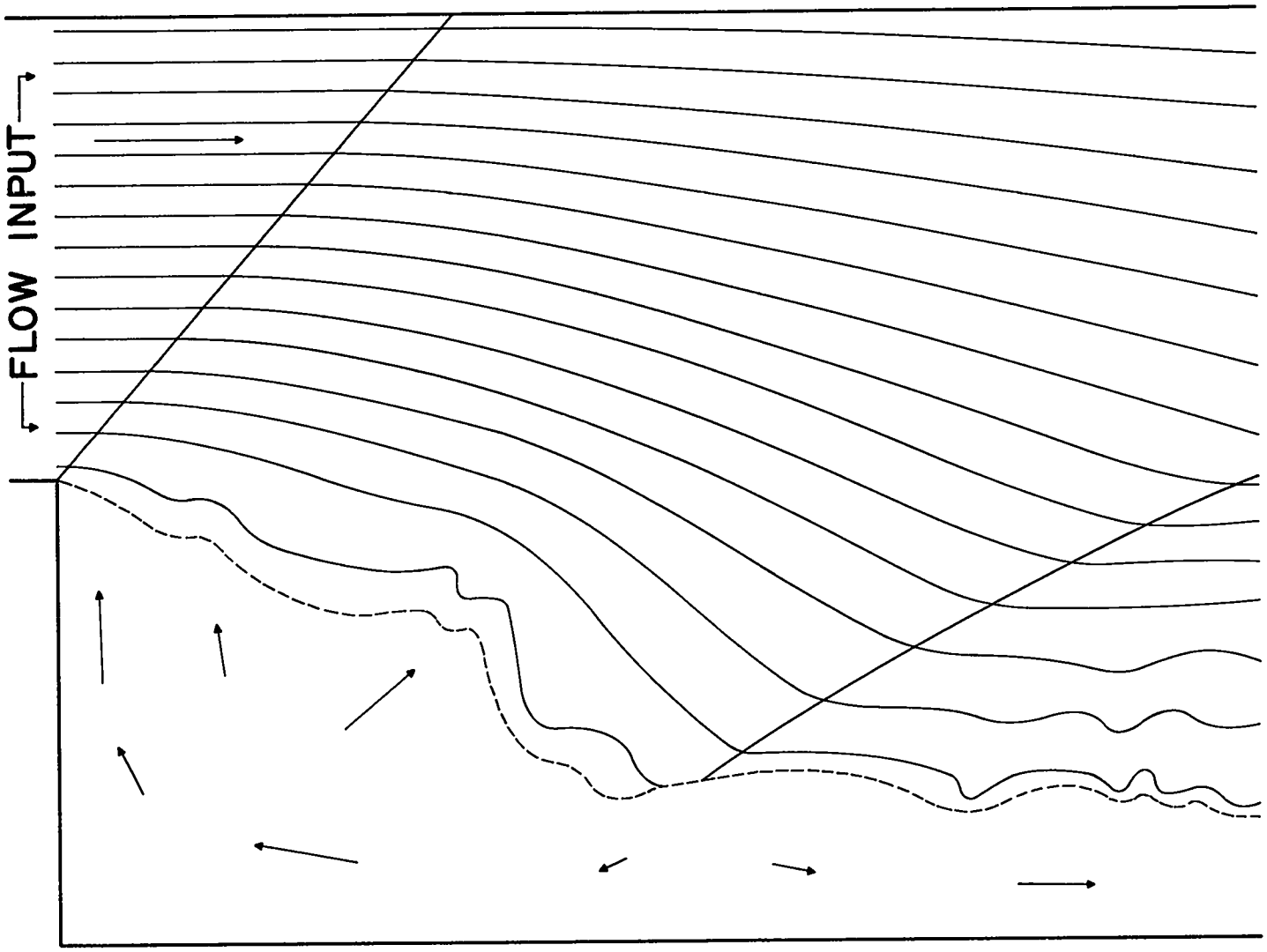

Fig. III-9 Configuration of the flow pattern at t = 70 for the calculation for helium, showing mass-point lines, region of turbulence with shock reflected therefrom, Mach line from corner, and some local-velocity vectors.

CHAPTER IV

INTERACTION OF A SHOCK WITH A DEFORMABLE OBJECT

A. Introduction

The encounter of a strong shock with a deformable object can result in a very complicated flow field which contains both diffraction and refraction processes. The PIC method calculations have been applied to a study of several idealized situations in which the object and the surrounding gas were both represented by the polytropic equation of state of a monatomic, non-viscous, nonconducting gas. The flow was two-dimensional, confined between rigid parallel channel walls. The object was rectangular in shape and attached to one of the walls; it and the surrounding gas were initially cold, so that the incoming shock strength was infinite.

In all calculations, units were scaled in such a way that the width of a computational cell was unit distance, and the material velocity behind the input shock was unity. The initial density of gas around the object was likewise unit mass per cell, while the object density was four times as great. Thus, the speed of the incoming shock was 1.33 and the density behind it was 4. The channel was 24 cells wide and the computation region in it was 50 cells long. The object was 10 cells wide in each case, but its length was variable. Along the left boundary there was input corresponding to constant conditions behind the shock.

B. Configurations of the Flow Fields

A typical interaction configuration is shown in Fig. IV-1. The object was a long rectangle, extending to the right side of the computation region. Positions of the interface and of the shocks were determined by reference to plots of the mass points, in a manner similar to that used in previous chapters.

A similar result is shown in Fig. IV-2. In this case the object length was twice its width. In addition to the features shown in Fig. IV-1, there is also shown the set of initially-horizontal mass-point lines. These are dashed in the turbulent-vortex region, where the flow pattern, as represented by the particle positions, is considerably more contorted.

C. Functionals of Motion

In the various computations reported in this paper, numerous functionals of the motion were calculated. For this set of calculations, it is appropriate that they be discussed in some detail, because they demonstrate several properties of the PIC method. In particular, several of the functionals can be compared with corresponding hand-computation results. Thus, for the problem whose late-time configuration is shown in Fig. IV-1, the vertical momentum of the entire flow field could be computed exactly by hand for times up to when a signal from the corner of the object reached one of the channel walls. The comparison is shown in Fig. IV-3. The effect of collision of a corner signal with the channel wall is clearly visible at $t = 26$.

Likewise, the circulation around the computation region could be hand-computed as a function of time. This was done for the shorter object, since the result shows a discontinuity in slope resulting from shock break-through at the back edge just after $t = 28$. The result is also shown in Fig. IV-3. The change in slope is clearly visible in the machine-computed results.

Finally, an approximate hand computation could be made of the kinetic and internal energies of the object; the results should be valid for early times after the encounter. The comparison is shown in Fig. IV-4 for the short-object calculation. The kinetic energy from the machine computation agrees with the hand-computed result nearly as well as do the circulation and vertical momentum. The time-wise lag in the internal energy curve has also been observed in various other PIC method calculations. It is easily explained by the nature of the finite-difference equations, and can be made smaller by a decrease in cell size.

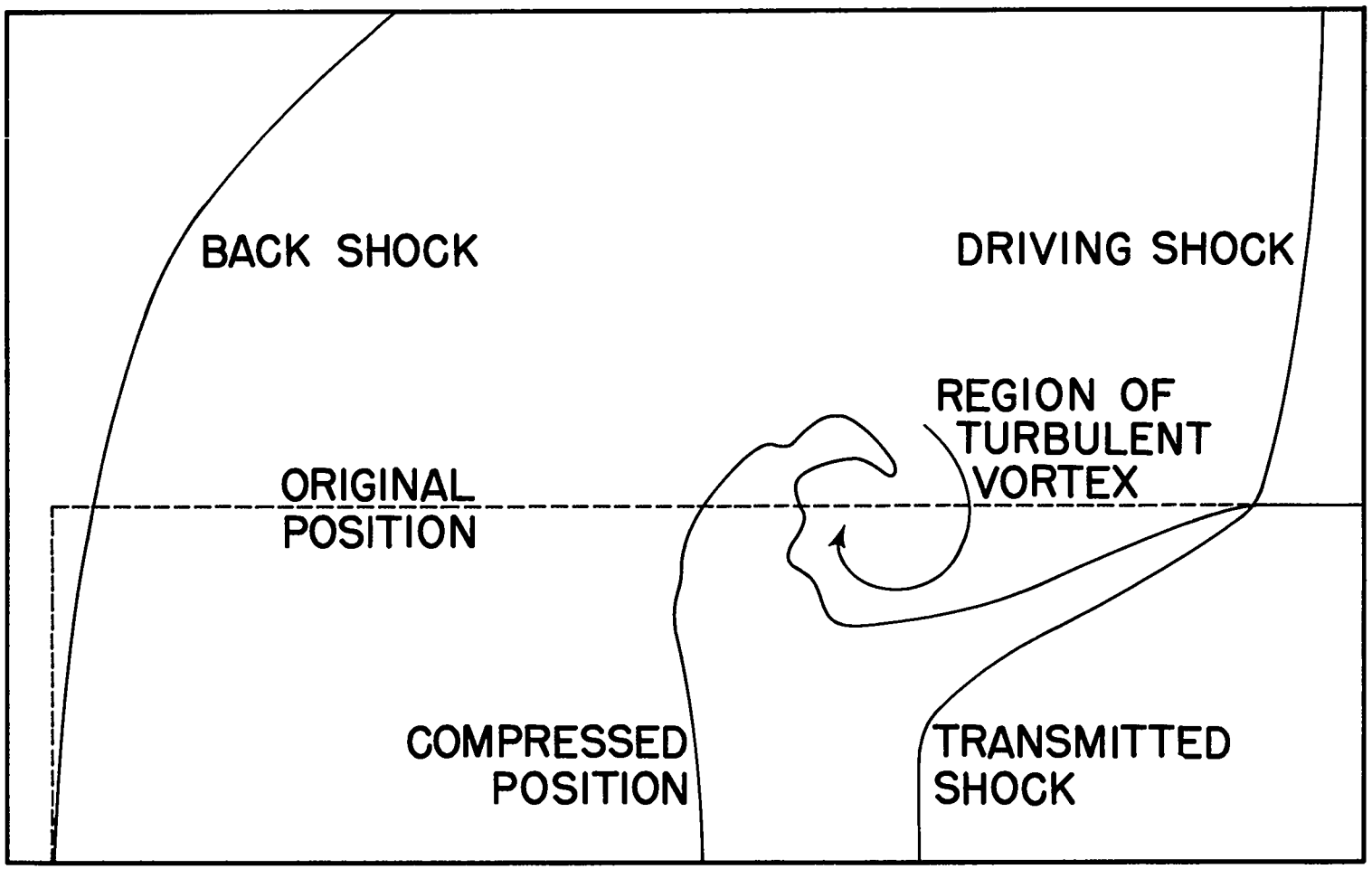

Fig. IV-1 Interface and shock positions at time t = 35 for the long object.

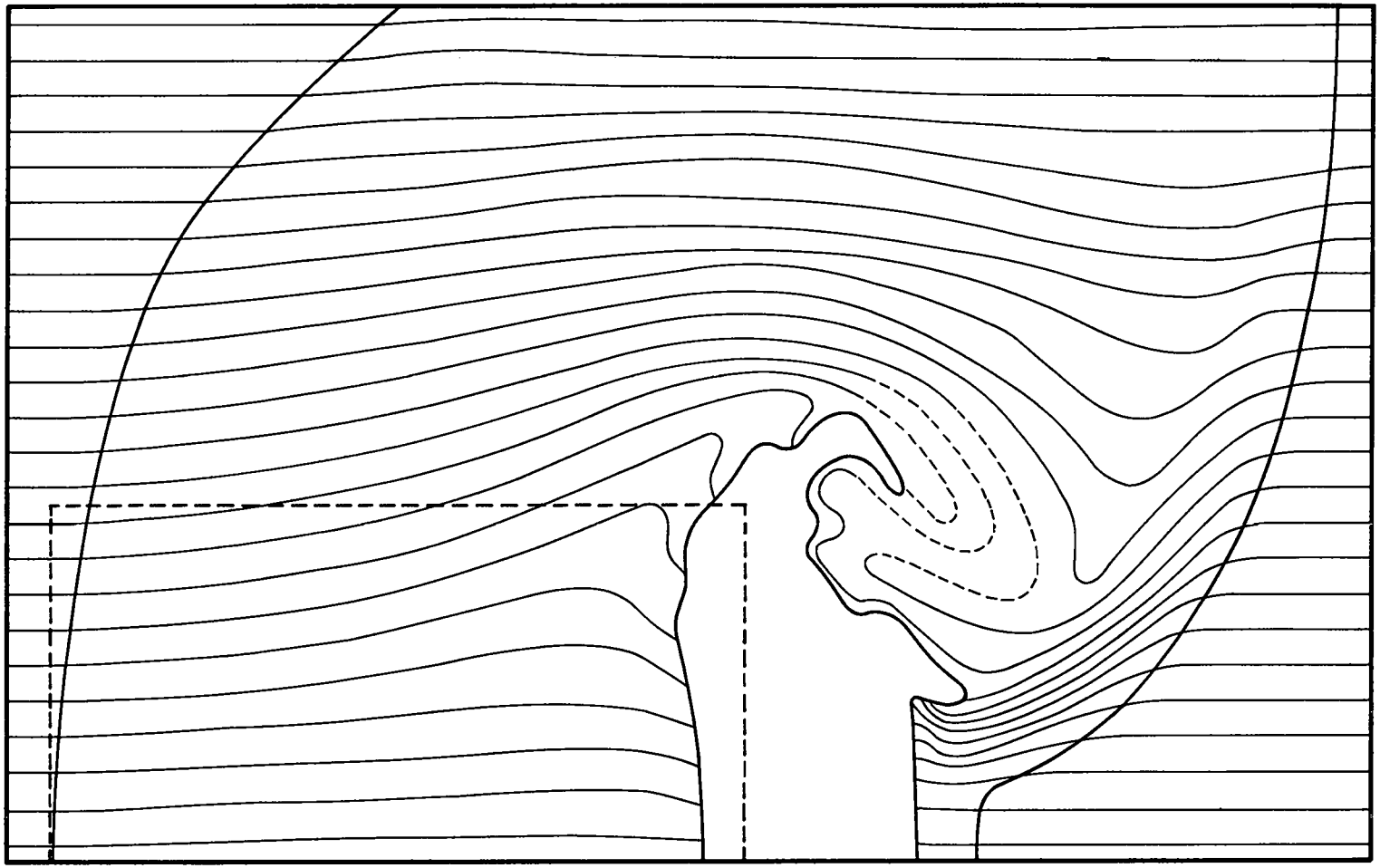

Fig. IV-2 Positions of the interface, shocks, and mass-point lines at time t = 35 for the shorter object.

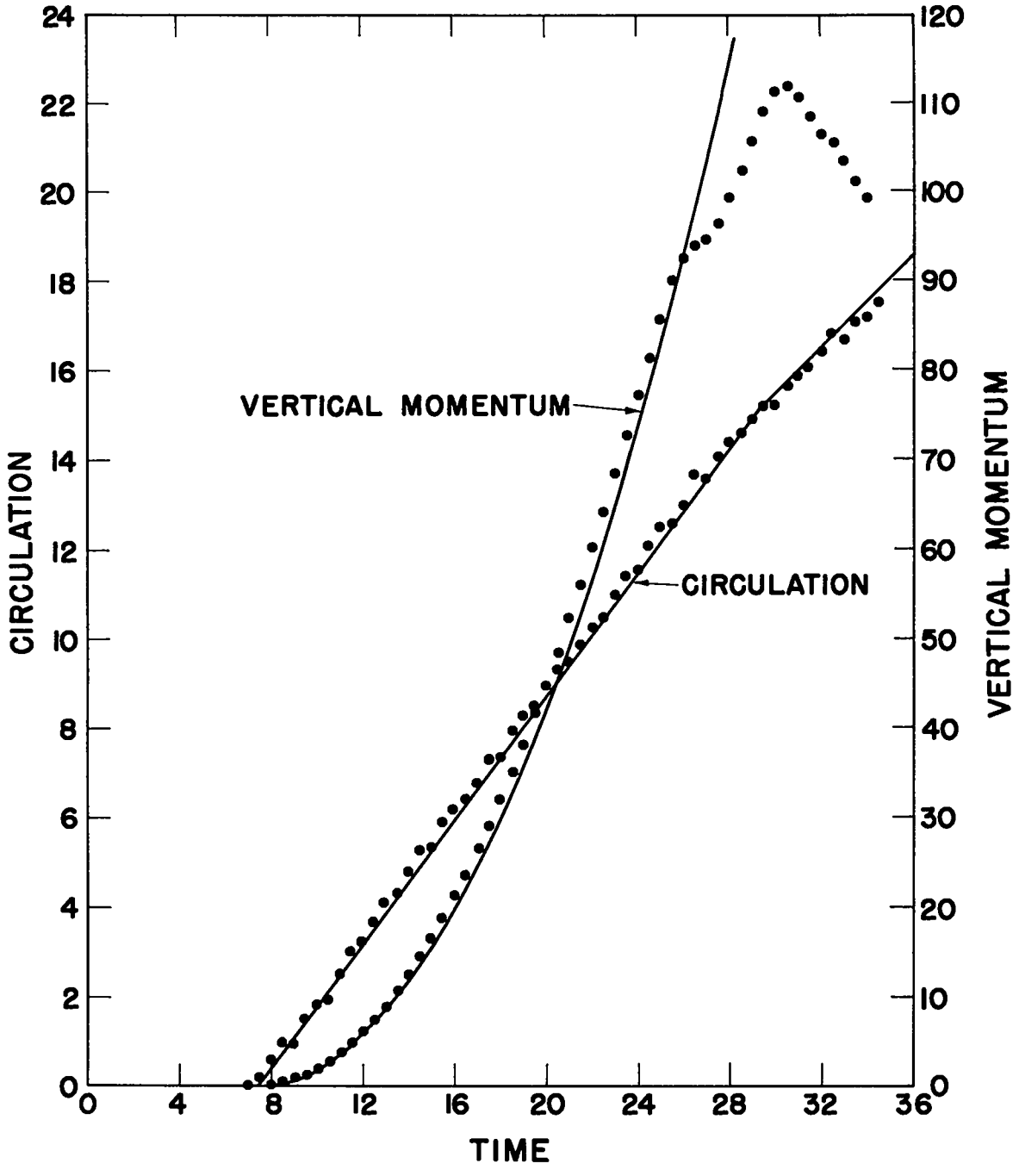

Fig. IV-3 Vertical momentum and circulation of the entire computation region as functions of time for the long- and short-object calculations, respectively. Datum points are from the machine computation; solid curves were hand-computed, using shock theory.

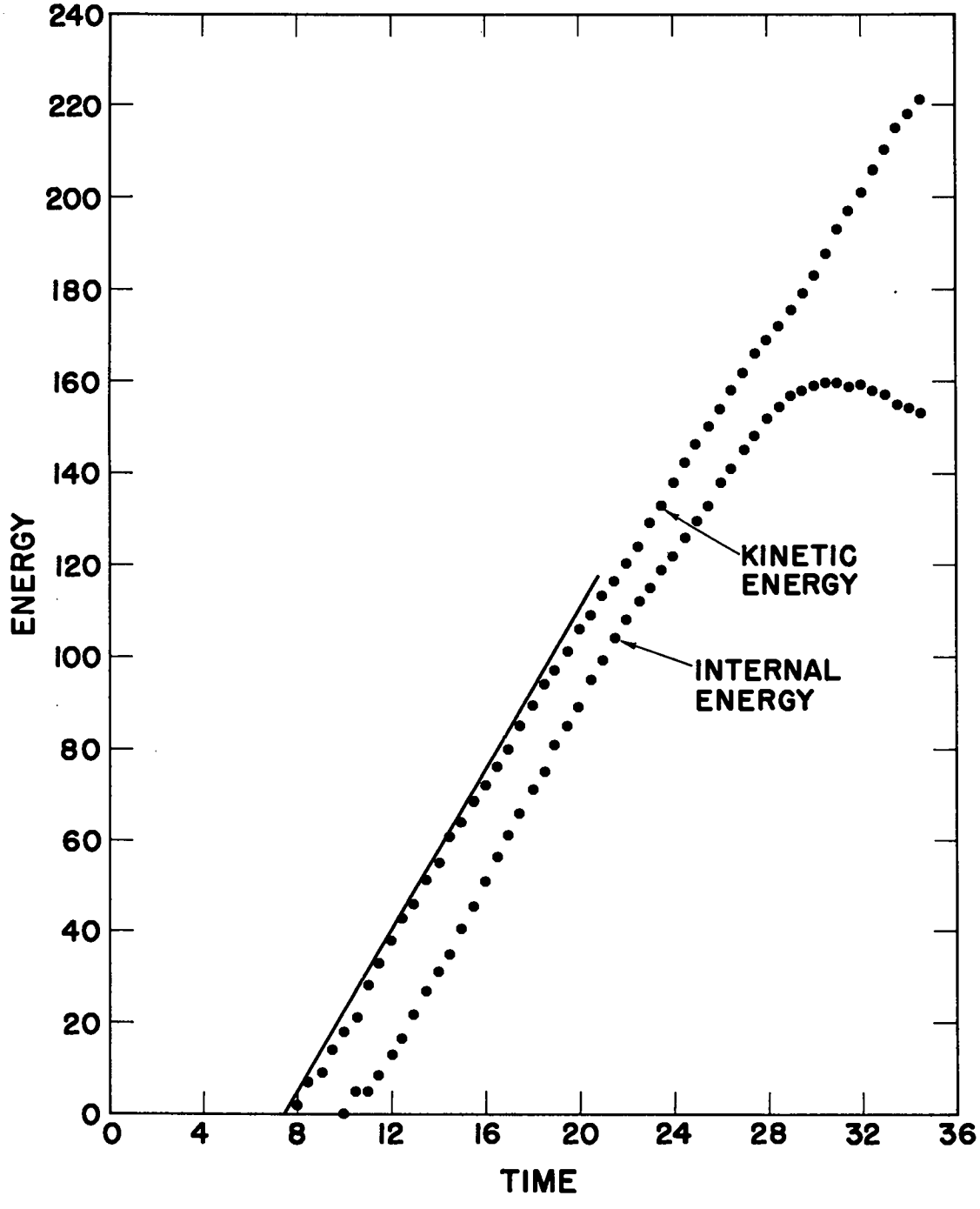

Fig. IV-4 Internal and kinetic energies of the object as functions of time for the short-object calculation. Datum points are from the machine computation; solid curve was hand-computed and represents both internal and kinetic energies.

CHAPTER V

HYPERSONIC SHEAR FLOW WITH PERTURBED INTERFACE

A. Introduction

We have used the PIC method to study the plane, two-dimensional interaction of two gases moving past a perturbed slip plane. The gases were confined between infinite, parallel, rigid walls; in cross section, the initial slip plane was approximately a low-amplitude sine wave with mean position halfway between the walls. The gases were initially cold (zero sound speed); the upper one was moving to the right and the lower one to the left, both parallel to the channel walls and with the same speed. Both gases were polytropic, nonviscous, nonconducting, and monatomic (specific heat ratio $\gamma = 5/3$).

The initial configuration was perfectly periodic along the channel, and it was assumed that subsequent interactions would preserve that periodicity. One period was divided into 1200 square cells—30 from wall to wall and 40 along the channel. The total number of mass points was 4800. Boundary conditions were reflective at the rigid channel walls and periodic at the ends.

Dimensions were scaled so that each cell was of unit width, the initial velocities were of unit magnitude, and the density of the upper gas was four units. Thus, the time unit was the time required for the undisturbed gas to move one cell. The initial perturbation of the slip line was always the

same—of unit amplitude and in the form of a step-function approximation (along cell boundaries) to a sine wave with origin at the left of the period. The parameter which was varied among calculations was R, the ratio of density of the upper to lower gases. The values studied were R = 1, 0.5, and 0.2, and the scaling laws allowed additional results to be derived from these, equivalent to R = 2 and 5.

B. The Interaction

Along the section of slip line with positive slope, the gases collided in the early stages. From this collision line, shocks proceeded into each gas; the gases were heated, and vertical kinetic energy was created. The shocks diverged and were carried along as shock pulses in undulating ribbon form, separated by rarefied regions of relative stagnation. In the early stages, a cavity opened along the section of slip line with negative slope.

Typical appearance of a well-developed configuration is shown in Fig. V-1 for the initial density ratio R = 1; the elapsed time was 30.7 units (the free-stream motion had carried the gas about three-fourths of a period). Mass-point lines shown for the upper gas were initially horizontal and evenly spaced; those for the lower gas were initially vertical (transverse to flow) and also evenly spaced. The dashed line shows the mean interface between the gases; initially, this approximately followed the dotted line. The central strip is rarefied and strongly turbulent as indicated by the admedian mass-point line of the upper gas. For R = 1, the configuration always satisfied the symmetry property that vectors reflected through the center point should change sign but not magnitude, while scalars remain unchanged.

In Fig. V-2 are shown the positions of the diverging shock fronts at various times for the problem with density ratio R = 0.2. These locations were defined by the positions at which the magnitude of vertical velocity

was one-tenth of the initial free-stream speed. The maximum and minimum heights of the two shock fronts are shown as functions of time in Fig. V-3. By t = 30, these shock fronts were moving at speeds of 0.36 and 0.14 cells per time unit in the upper and lower gases, respectively.

In addition to the two diverging shock-pulse ribbons, there was a central region of rarefaction wherein both gases had dropped to about one-third normal density at late times. In Fig. V-4 is shown the compression as a function of height above lower channel wall, at time t = 30, for the problem with density ratio R = 0.2. These compressions were obtained in the computation as cellwise quantities, "quantized" by integral numbers of particles in each cell, and have been smoothed in the plots.

The distinction between the diverging ribbons and the central rarefaction region is also strongly indicated by the vertical profiles of specific internal energy. One of these is shown in Fig. V-5 at time t = 30, at channel midlength, for the density ratio R = 0.2 (corresponding to the upper part of Fig. V-4). The ribbon temperature was slightly higher than that behind a theoretical plane shock of this speed. (A shock speed of 0.36 would indicate, with $\gamma = 5/3$, a vertical material speed of 0.27—which is close to the observed value—but this in turn leads to a specific internal energy of 0.37.) The explanation lies in the fact that the shock was actually oblique on its left face, where the shock speed was greater relative to the material.

Energy was transferred from the denser to lighter gas at a rate which is roughly proportional to $(1 - R)/R$ in the range of density ratios considered. This transferal was a secondary effect, in that the rate remained negligible for some time and then gradually increased.

Another secondary energy effect was the production of vertical kinetic energy. The rate of production roughly equaled the rate at which energy was transferred to the lighter gas in the case R = 0.2, but was somewhat

larger for larger values of R. Crude calculations using simple shock theory suggest that the rate of production of vertical kinetic energy in the upper gas should be proportional to $(1 + \sqrt{R})^{-3}$ for all values of R. This crude calculation agrees surprisingly well with the results of the full machine calculations for early times. In Fig. V-6 is shown the vertical kinetic energy in the upper gas for five different densities of the lower gas. (The curves for R = 2.0 and 5.0 were obtained by scaling the energies of the lower gas from the runs with R = 0.5 and 0.2, respectively.) Also shown as a set of isolated points at t = 10 are the values of $45(1 + \sqrt{R})^{-3}$, the constant of proportionality having been chosen to fit the value for R = 0.2. Variation in the accuracy of agreement at earlier times is consistent with the expected variations in the finite-difference results. The late-time drop in the curve for R = 0.5 arises from collision of the shock with the upper channel wall. The other problems were not run far enough for collision because of the machine time involved.

A primary energy effect was the production of internal energy. In Fig. V-7 is shown the internal energy of the upper gas as a function of time. The inset, at the same scale, shows the early-time section of the curves as the data came from the machine. The contortions can be traced to a fictitious effect of the finite-difference technique; these have been smoothed slightly in the full curves.

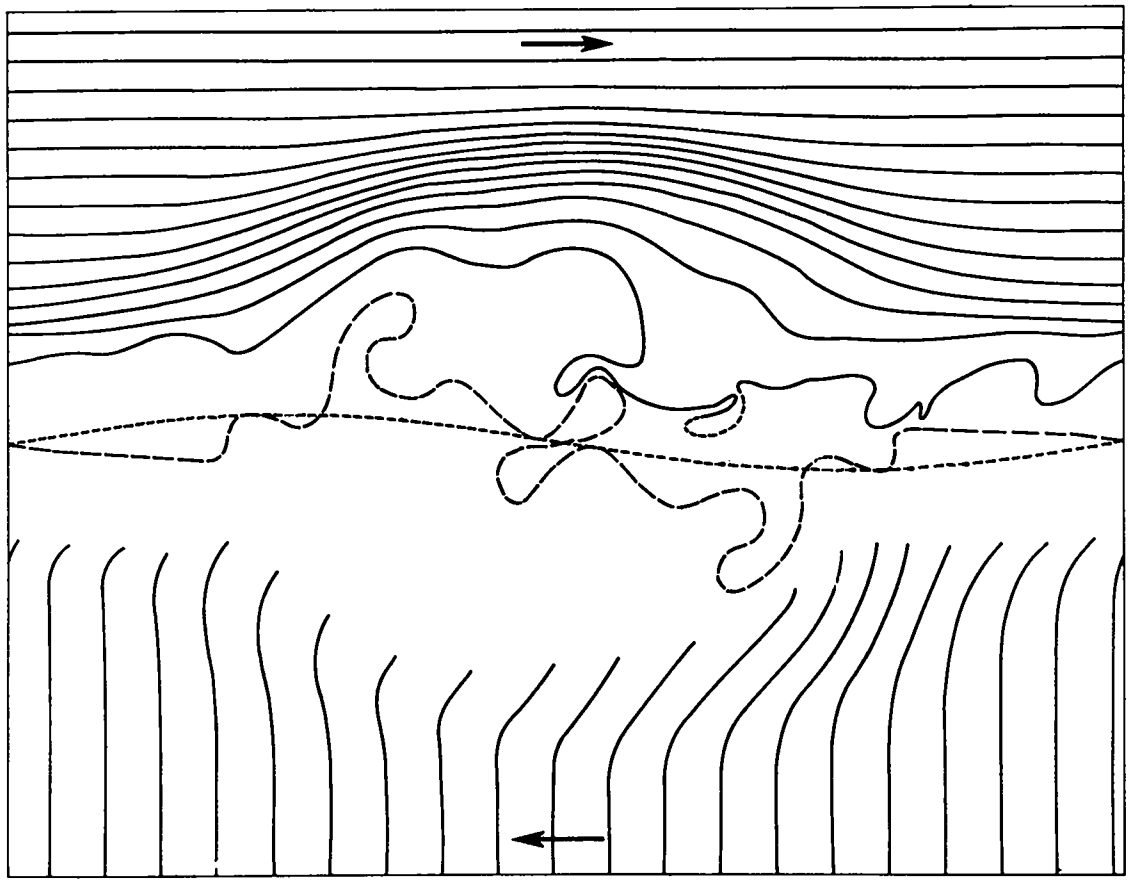

Fig. V-1 Configuration at time 30.7 units for problem with R = 1. Upper gas shows longitudinal mass-point lines; lower gas shows transverse mass-point lines. Dashed line is interface position which was originally along the dotted line. Locus of ends of lower mass-point lines delineates normal density isopycnic.

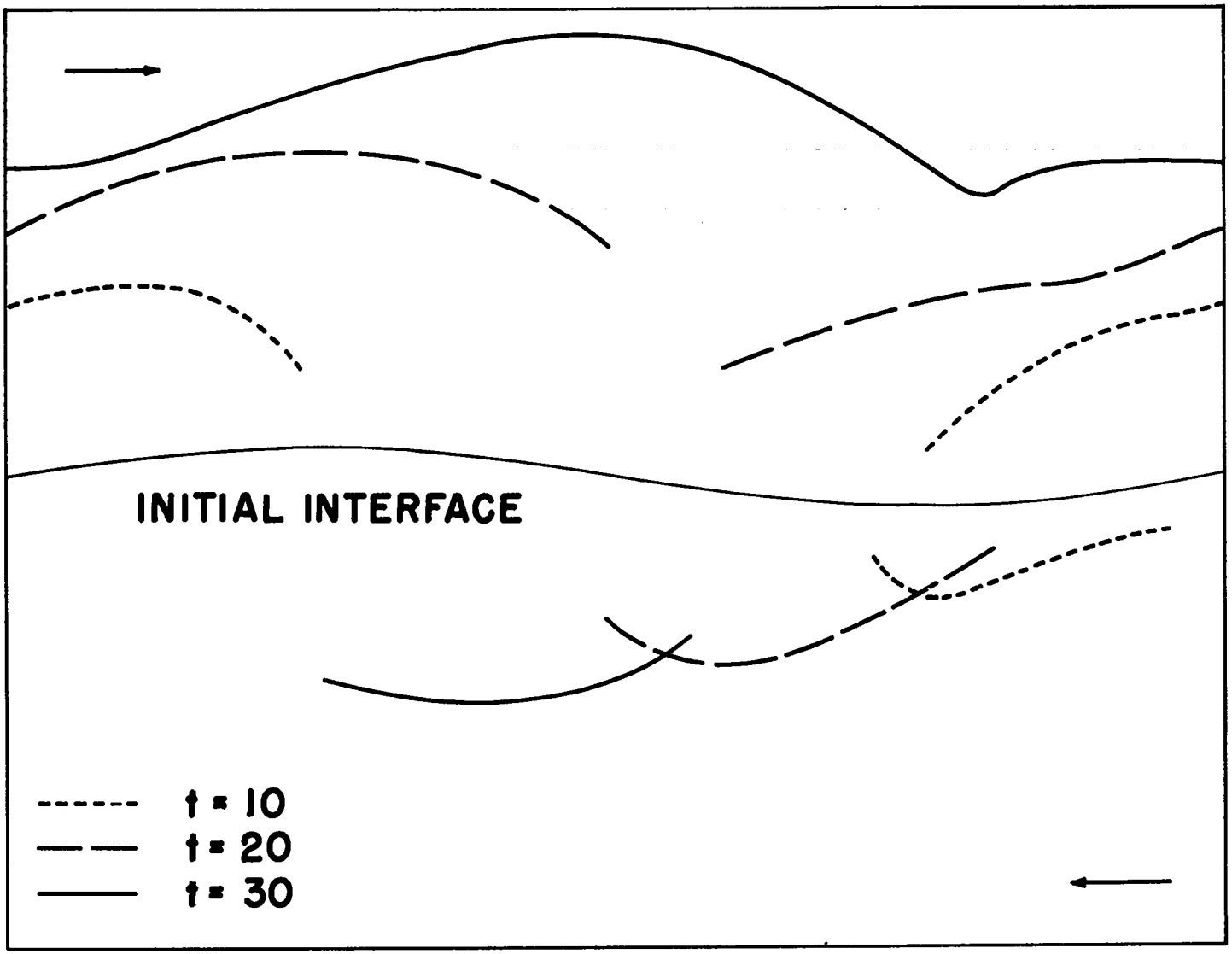

Fig. V-2 Position of the shock fronts at various times for the problem with R = 0.2.

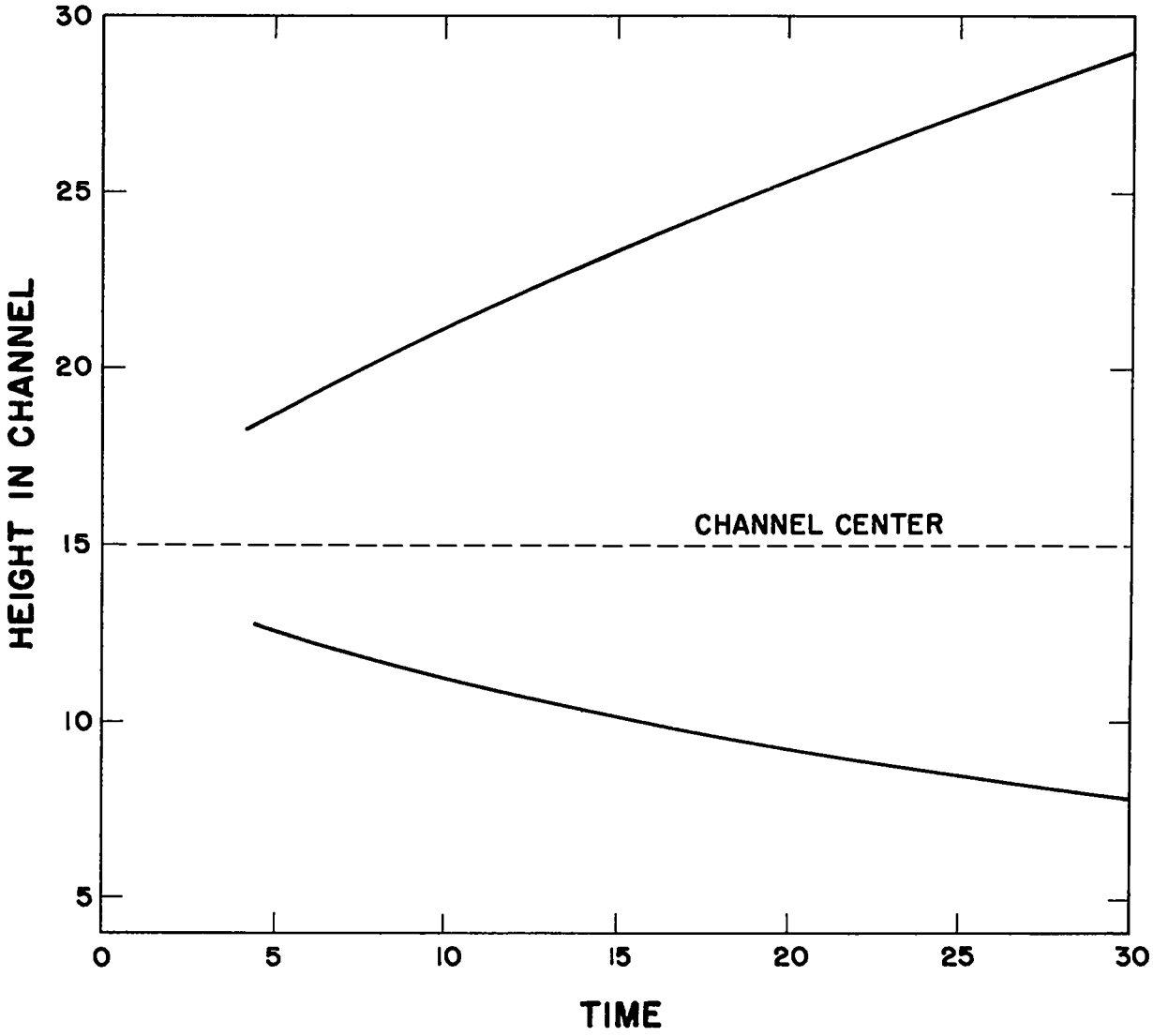

Fig. V-3 Position of the maximum and minimum shock heights as a function of time for the problem with R = 0.2.

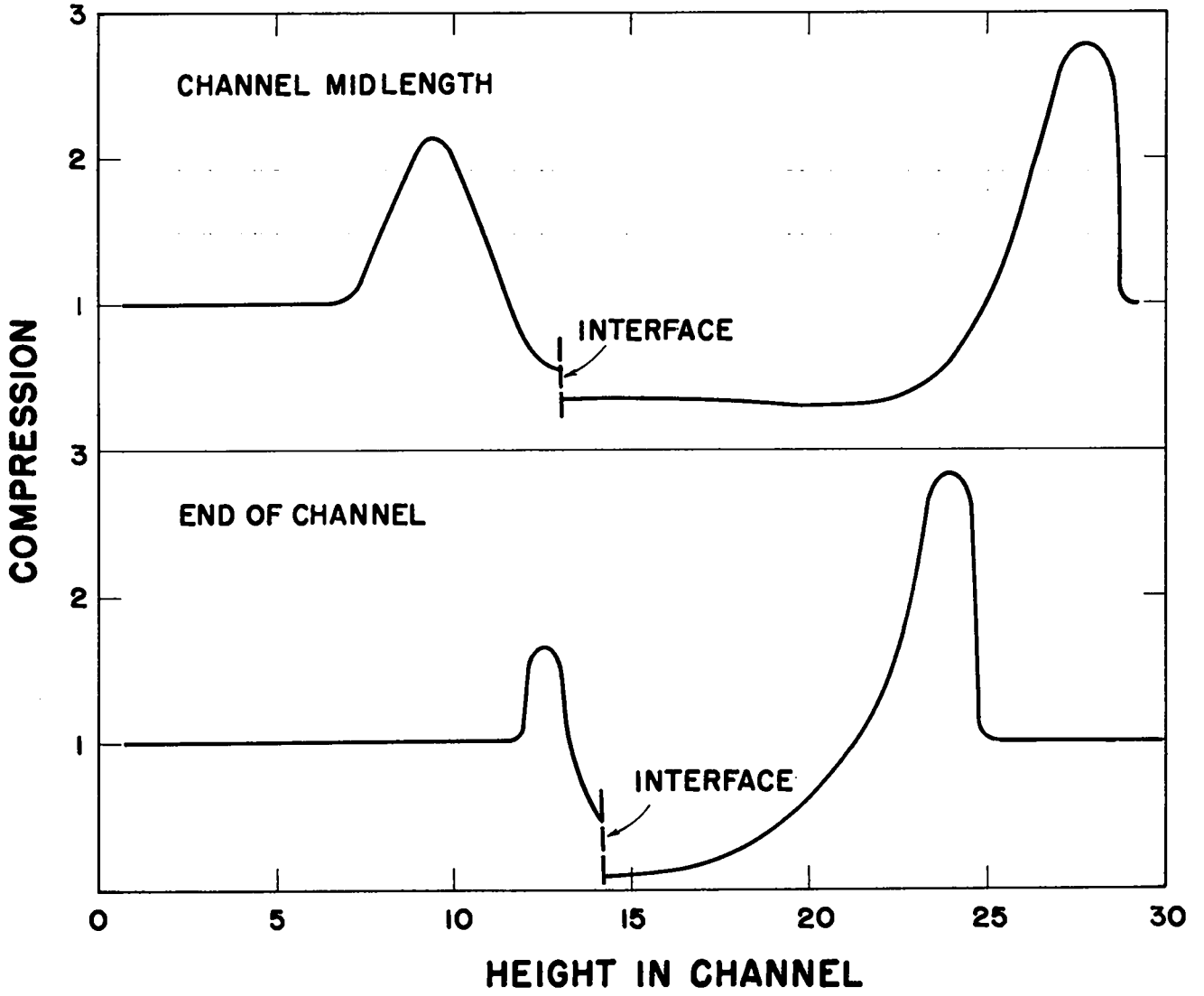

Fig. V-4 Vertical compression profiles at channel end and midlength at time 30 units for the problem with R = 0.2.

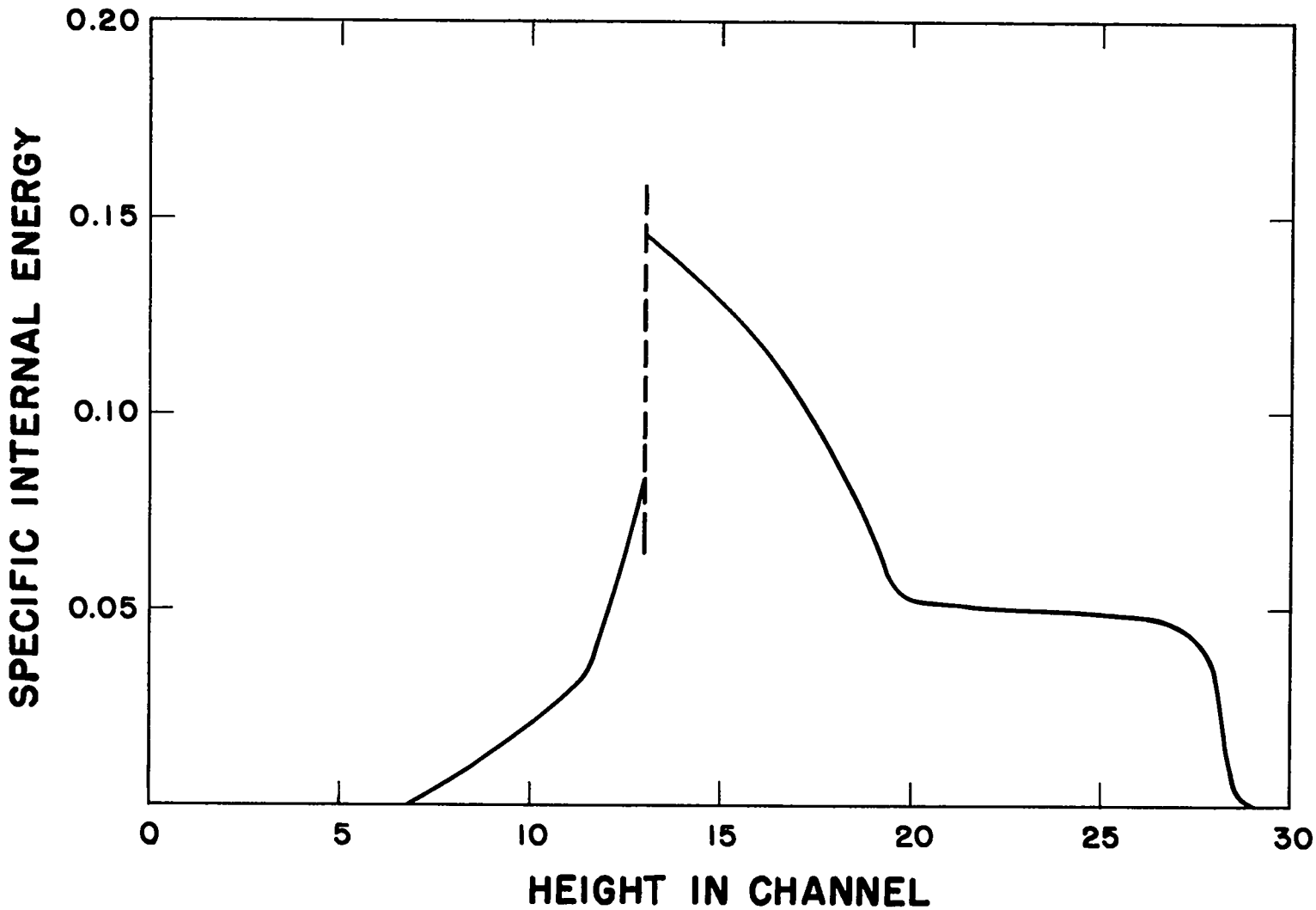

Fig. V-5 Vertical internal energy profile at channel midlength at time 30 units for the problem with R = 0.2.

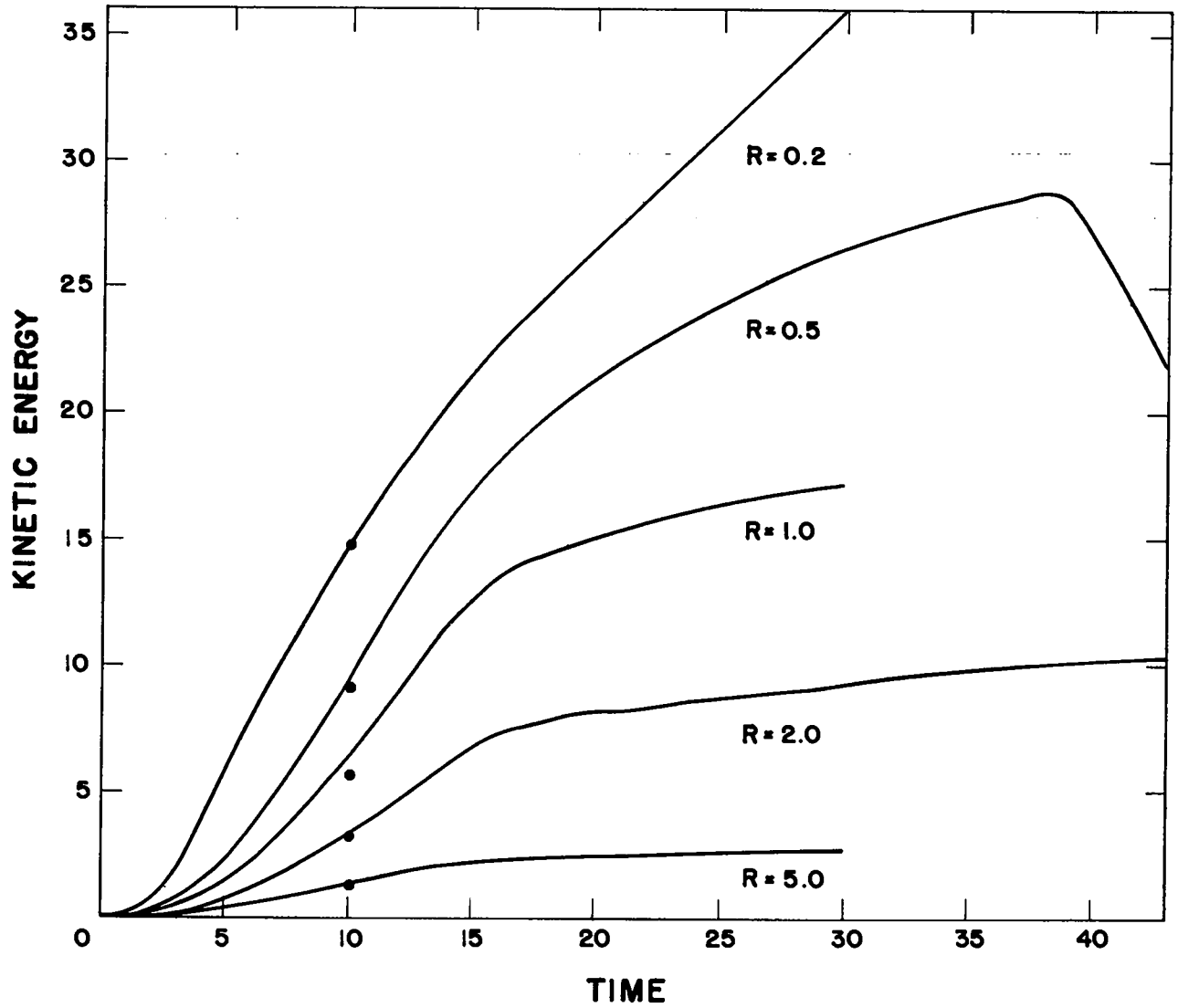

Fig. V-6 Vertical kinetic energy of the upper gas as a function of time for various values of the density ratio. Isolated points near each curve are values of $45(1 + \sqrt{R})^{-3}$.

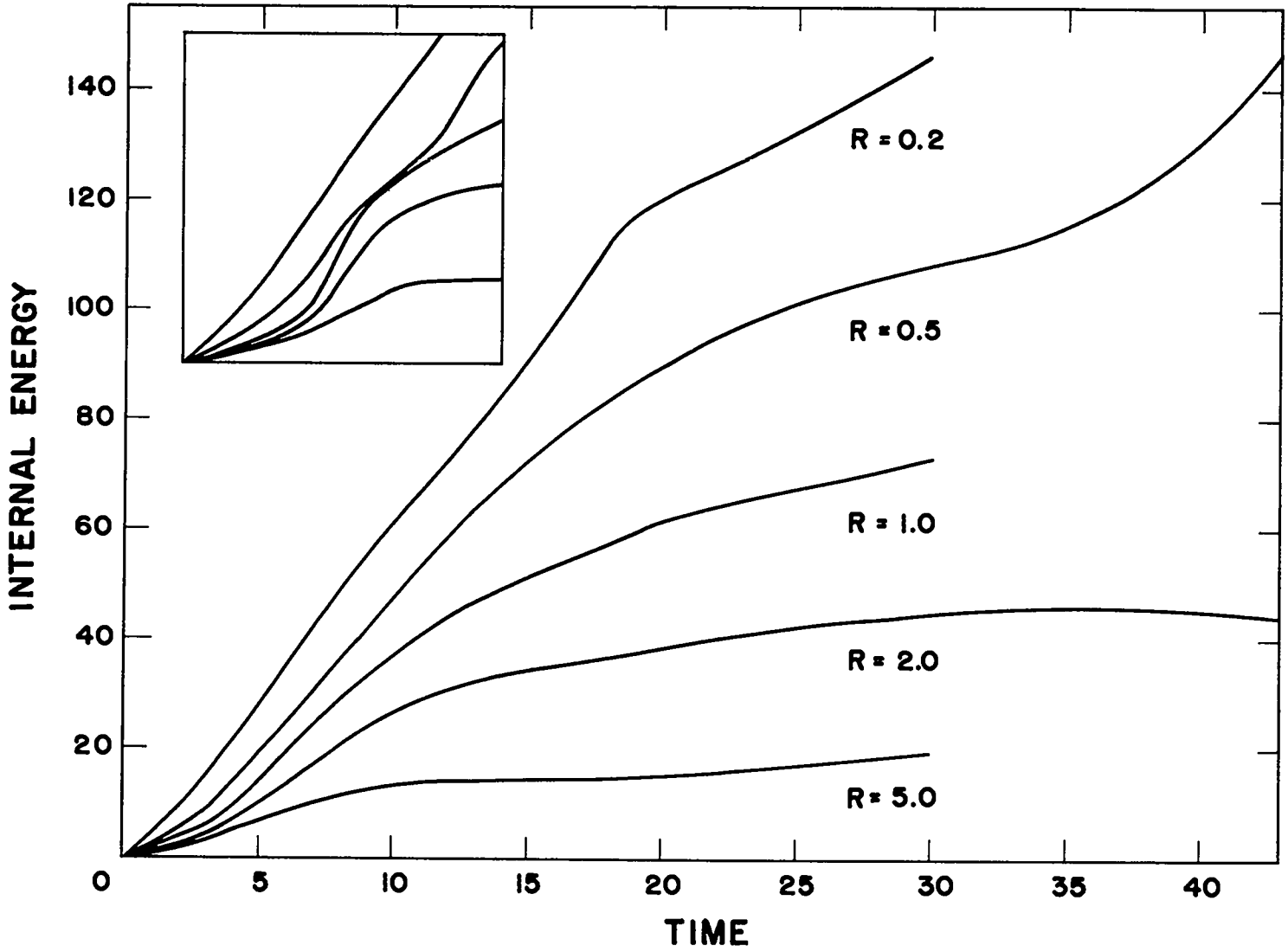

Fig. V-7 Internal energy of the upper gas as a function of time for various values of the density ratio. Inset, at the same scale, shows the unsmoothed appearance at early times.

CHAPTER VI

TAYLOR INSTABILITY

The PIC method has been applied to problems involving the instability of irregular gaseous interfaces subjected to normal acceleration. A typical sequence of configurations is shown in Fig. VI-1. The calculations were performed in cylindrical coordinates, with the axis forming the left boundary of the picture; the other boundaries were rigid and reflective. The two gases were initially cold, nonviscous, nonconducting and polytropic, with specific heat ratio $\gamma = 2$. The initial boundary between them, as shown in Fig. VI-1, was perturbed to a square-tooth shape. Smaller perturbations were not studied because of lack of resolution; larger ones could not be studied because of the effects of boundary signals. Acceleration was supplied by an applied pressure in the empty cells; the procedure is discussed in Chapter I, Section B-6. As mentioned there, the "empty" region behaves as though it were filled by a very hot gas at very low density. The pressure is finite (specified) but the sound speed is very high, so that the pressure remains homogeneous. It is assumed that this "gas" is backed by an infinite reservoir, so that its pressure is constant in time. Thus it is expected that the applied-pressure boundary will always be unstable.

A shock passing through the upper gas eventually crosses the boundary between gases. The resulting compression in the vicinity of the boundary

(by a factor of three for $\gamma = 2$) initially decreases the perturbation amplitude. If the ratio, R, of density of lower gas to that of upper gas is greater than unity, then it is expected that the perturbation amplitude will subsequently grow. For $R \leq 1$, the surface should be stable.

In each of the calculations, there were 1200 square computational cells; units were scaled so that each was of unit width. The applied pressure was such as to give a material velocity behind the initial shock of 0.1 cell per unit time.

In Fig. VI-1 there is shown a sequence of configurations of the upper gas for the calculation with density ratio $R = 2$. Corresponding configurations are shown in Fig. VI-2 for density ratio $R = 0.5$. In the latter case, the lower surface was stable, but had changed phase by late time. In the former calculation the lower-surface perturbation amplitude had increased back to its original amount by time $t = 230$. Subsequently, however, the amplitude remained nearly constant, while the shape of the interface changed. In both cases, the upper surface had become perturbed; the amplitude increased most in the calculation with $R = 0.5$, in which there was the greatest acceleration of that surface.

Results of a similar, but more extreme, pair of calculations are shown in Figs. VI-3 and VI-4. The initial configuration was the same as before in both cases, but is not shown in Fig. VI-3 because of overlap in drawing the later configuration. In the first of this pair, the density ratio was $R = 20$; by time $t = 230$, the lower-surface amplitude had increased to three-halves its original amount, and the upper surface was considerably irregular. For the case $R = 0.05$, there was again a phase change in the lower-surface perturbation. The shape of the surface was quite distinctive. The upper gas remained quite thick; the upper surface is not shown, again because of overlap with earlier lower-surface positions, and because only by the last

time had that surface become appreciably perturbed.

In one additional calculation, the lower gas was omitted and the perturbation placed along the upper surface of the upper gas, adjacent to the applied pressure. A sequence of interface configurations is shown in Fig. VI-5. Some small droplets which broke from the top of the axial spike are not shown. The lowest configuration in the drawing is displaced downward from its true position to prevent overlap.

It is unfortunate that none of these results could be compared with experiment or other theory. Qualitatively, the results appear reasonable; it is thought that they also have quantitative accuracy, to some extent.

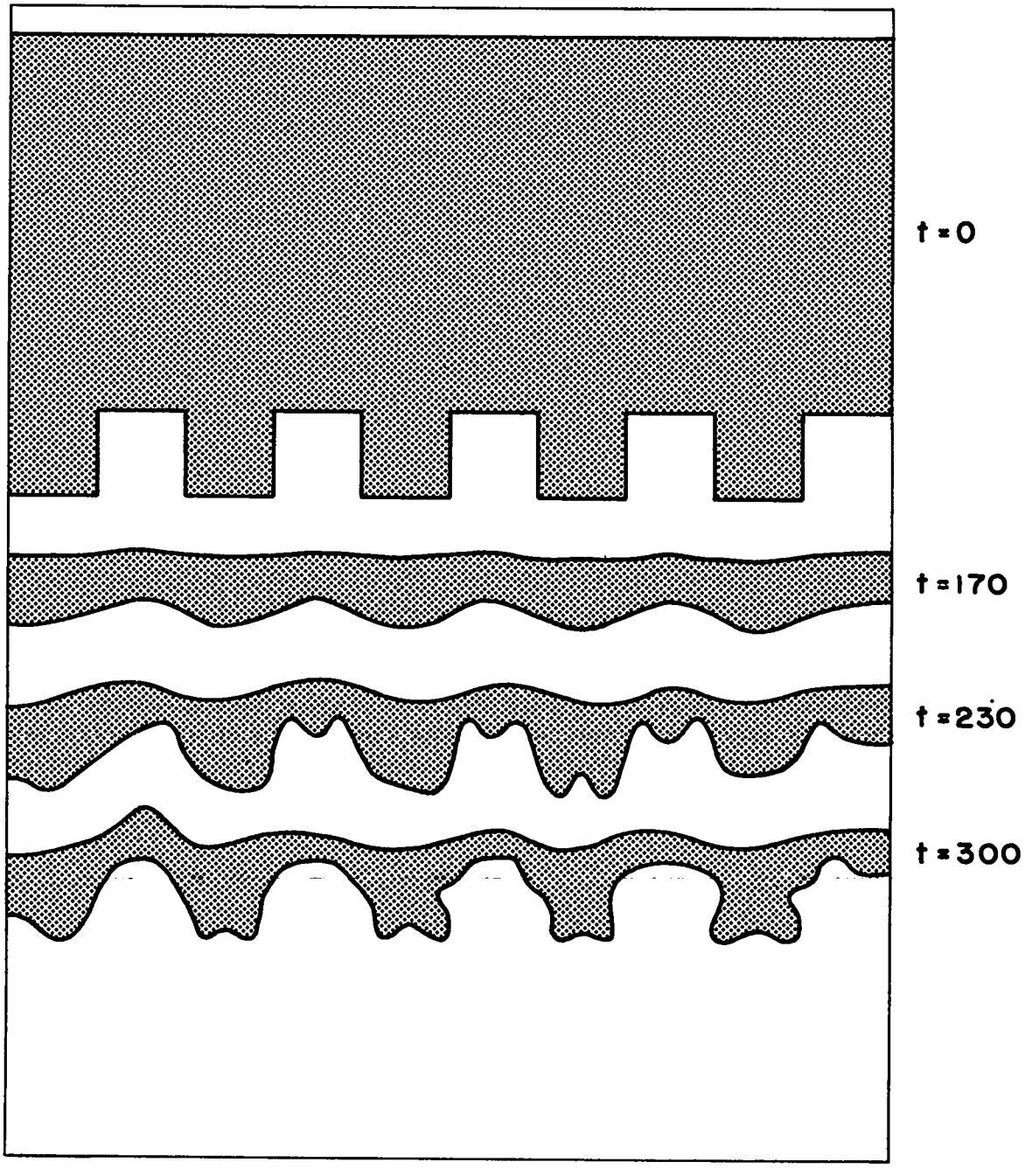

Fig. VI-1 Sequence of configurations of the upper gas for calculation with density ratio R = 2.

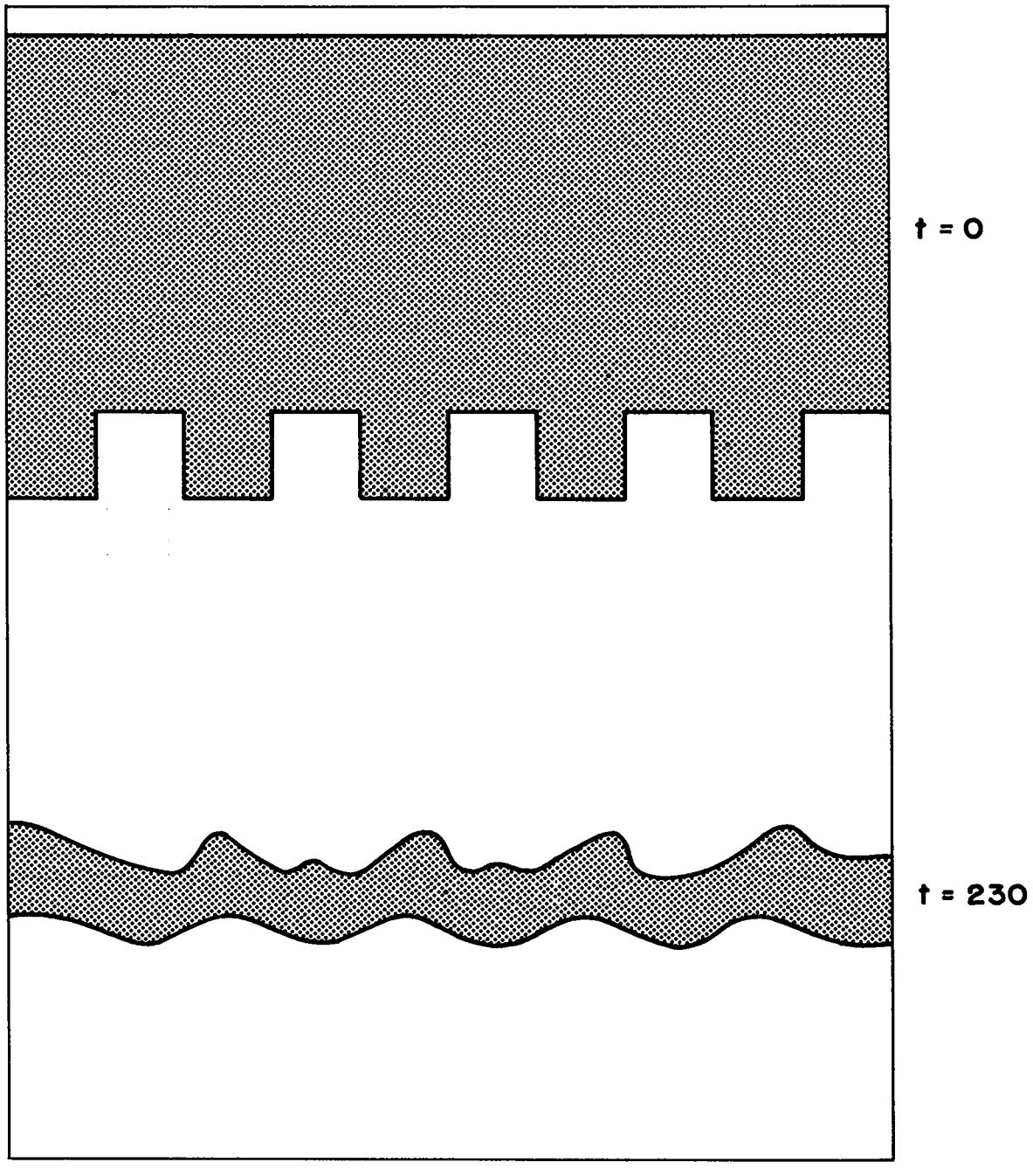

Fig. VI-2 Two configurations of the upper gas for the calculation with density ratio R = 0.5.

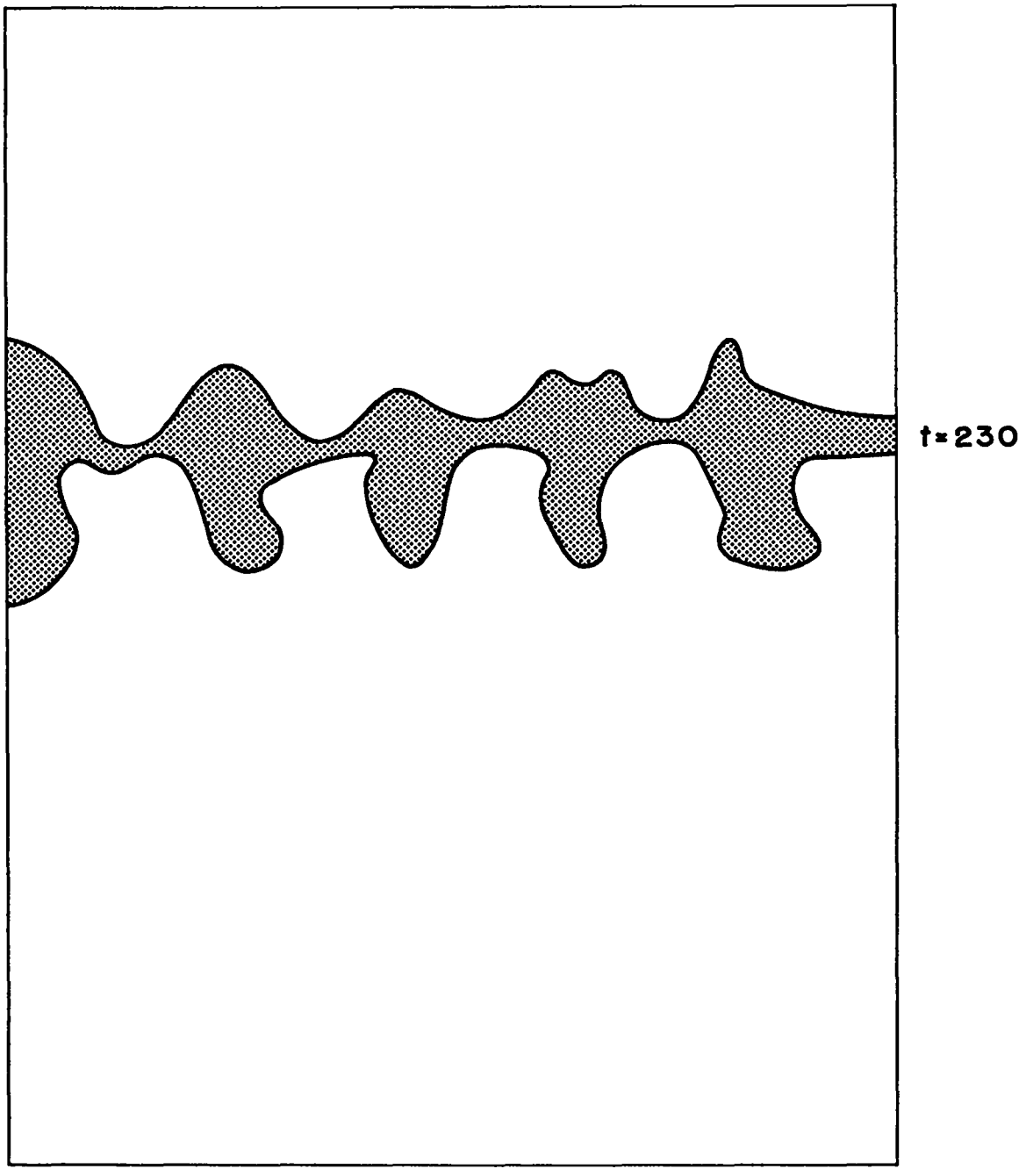

Fig. VI-3 Late-time configuration of the upper gas for the calculation with density ratio R = 20.

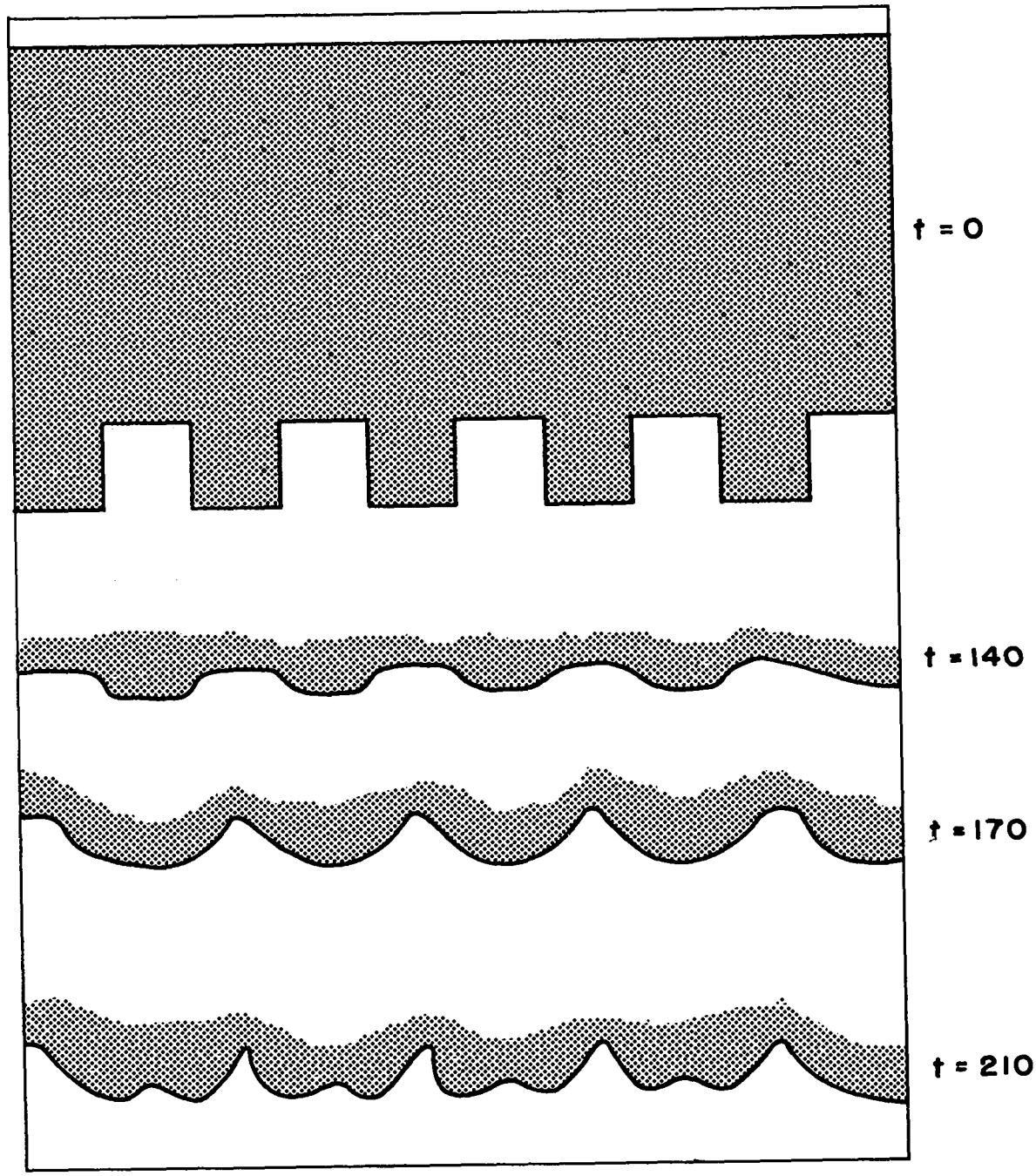

Fig. VI-4 Sequence of configurations of the upper gas for the calculation with density ratio R = 0.05. Upper surface is shown only for t = 0.

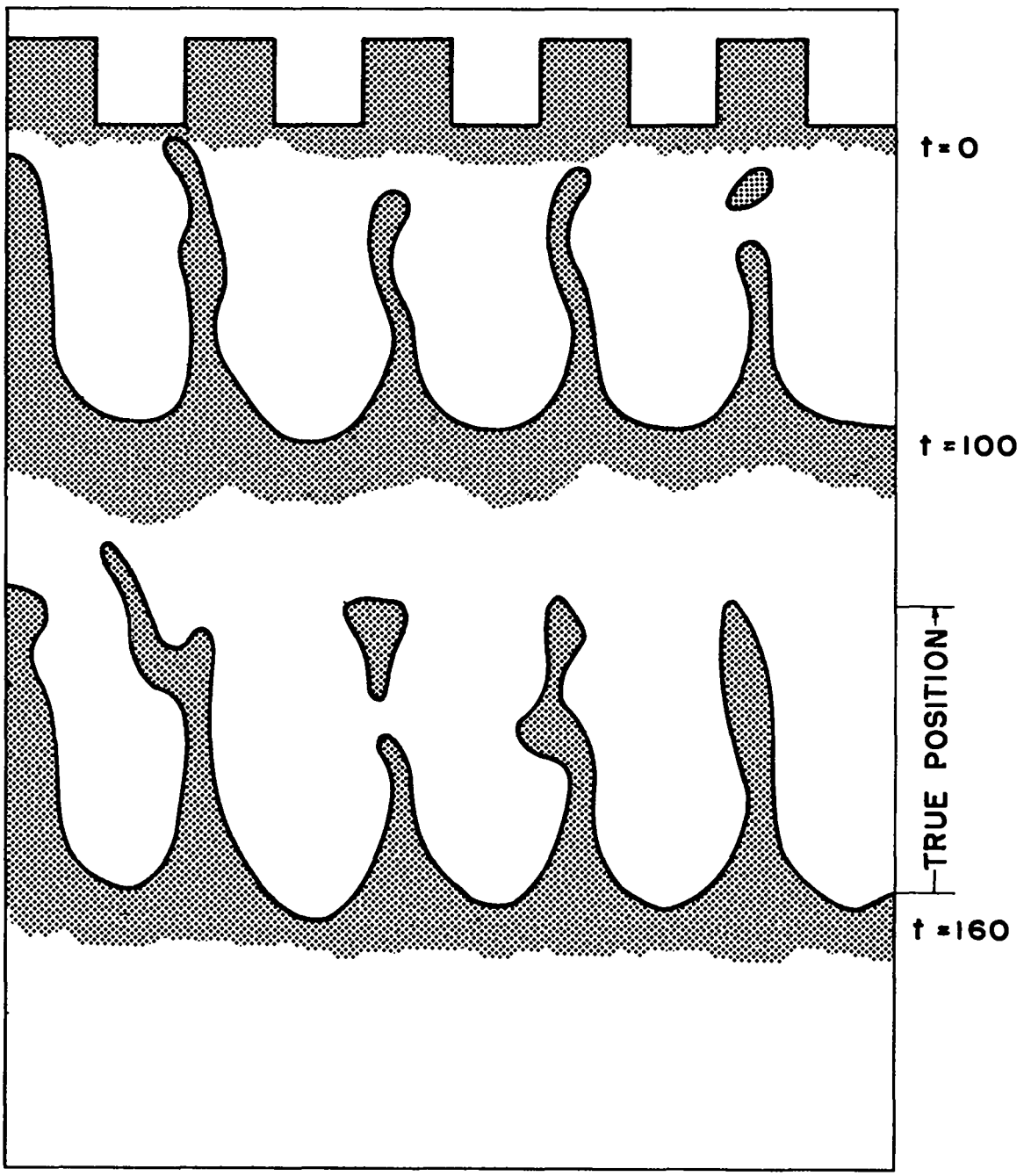

Fig. VI-5 Sequence of configurations of the upper gas surface for the calculation with applied-pressure-interface perturbation. Lowest configuration is displaced as shown to avoid overlap.

CHAPTER VII

VISCOUS-FLOW CALCULATIONS

A. Introduction

The procedure outlined in Chapter I, Sec. C, has been applied to several problems concerning the flow of a viscous, heat-conducting, polytropic gas. Results of several of the calculations are presented here.

The gas in each case was air for which we took $\gamma = 1.4$, $A = -2/3$, $B = 1.9$. The first viscosity coefficient was assumed to vary with specific internal energy (hence with temperature) according to the relation $\mu = \mu_0 I^n$, where the exponent was a constant. (In Sec. B below, n = 0.5; in Sec. C, n = 0.) In each case, the channel wall was allowed to be conducting and held at a fixed temperature. There were ten cells across the channel and three columns of cells along one period of the channel. In each case, the flow was actually one-dimensional, but results were improved by along-channel averaging.

B. Couette Flow

Initially, the gas was at rest and at uniform density, ρ_0, and specific internal energy, $I_0 = 1.0$. (The value of I at the walls was held fixed at that value.) At time t = 0, the lower wall (at y = 0) was impulsively accelerated to velocity u_0, and thereafter moved at that constant rate.

It can be shown that under these circumstances the final (steady-state) maximum value of I should be

$$I_m = I_0 + \frac{u_0^2}{8B}$$

Thus, we may distinguish between low-velocity and high-velocity Couette flow according as u_0^2 is distinctly less than or greater than $8BI_0$. In the former case, the temperature (hence the density) remains nearly uniform across the channel. In the latter, the central temperature is large and most of the mass is confined to narrow bands at the walls.

At first we placed the particles in an orderly fashion, four per cell, one at the center of each quadrant. In the low-velocity calculations, the results were satisfactory because the density changes were so small that there were no vertical particle crossings. In the high-velocity calculations, however, such functionals of motion as total kinetic energy of the system, plotted as a function of time, showed discontinuities in slope. These occurred whenever a row of particles all simultaneously made a vertical crossing. An alternate procedure in particle placement was found to be considerably more satisfactory: Initially, the positions of the four particles in each cell were generated at random. As a result, the functionals of motion were much smoother and in better agreement with analytical calculations.

Simple tests of the calculation procedure produced results whose accuracy is as good as expected with the coarse mesh used. Some plots of velocity and specific internal energy are shown as functions of height above lower channel wall in Figs. VII-1 and VII-2. This was a low-velocity case; $u_0 = 1.0$. The results of a high-velocity Couette flow calculation ($u_0 = 10$) are shown in Fig. VII-3 for a late time. The five-times-compression curve

should rise to a value of 36 at each side to maintain constant pressure. It was apparent that the channel center would never cool to the theoretical limit in this calculation. The reason could be traced to a fault of the boundary conditions at the walls. It was assumed that there the specific-internal-energy gradient was the value obtained by subtracting from the value in the first cell the assigned wall value and dividing the result by half the cell width. The gradient thus calculated was much less than the true value; thus, a quadratic fit procedure was tried for calculating the gradients. The result showed considerably better agreement in the value of maximum temperature.

Even though the final density was far from uniform, the along-channel momentum from the machine calculation asymptotically approached a value which was very close to that obtained analytically as a result of the simple assumption that the density and velocity gradients were constant across the channel.

C. Poiseuille Flow

The initial conditions were the same as in Sec. B. At time $t = 0$, a body acceleration was applied: $g = 0.04$. An approximate analytical solution was obtained for the problem, and comparisons with the machine-computed results are shown in Figs. VII-4, VII-5, and VII-6. The discrepancies are of the same magnitude as the expected error in the approximate solution.

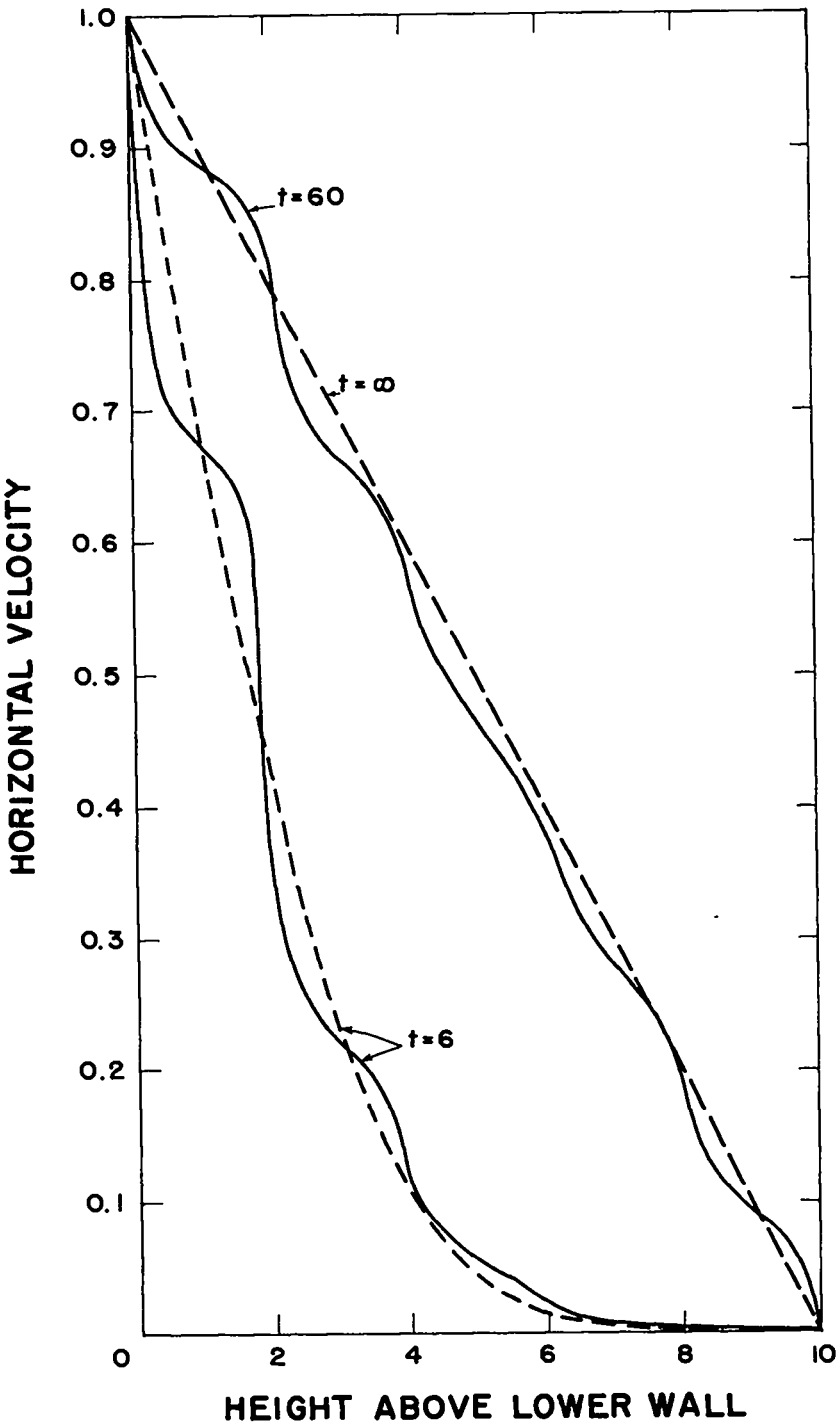

Fig. VII-1 Solid curves show machine-calculated velocity as a function of height for low-velocity Couette flow. Dashed curves are analytical solutions.

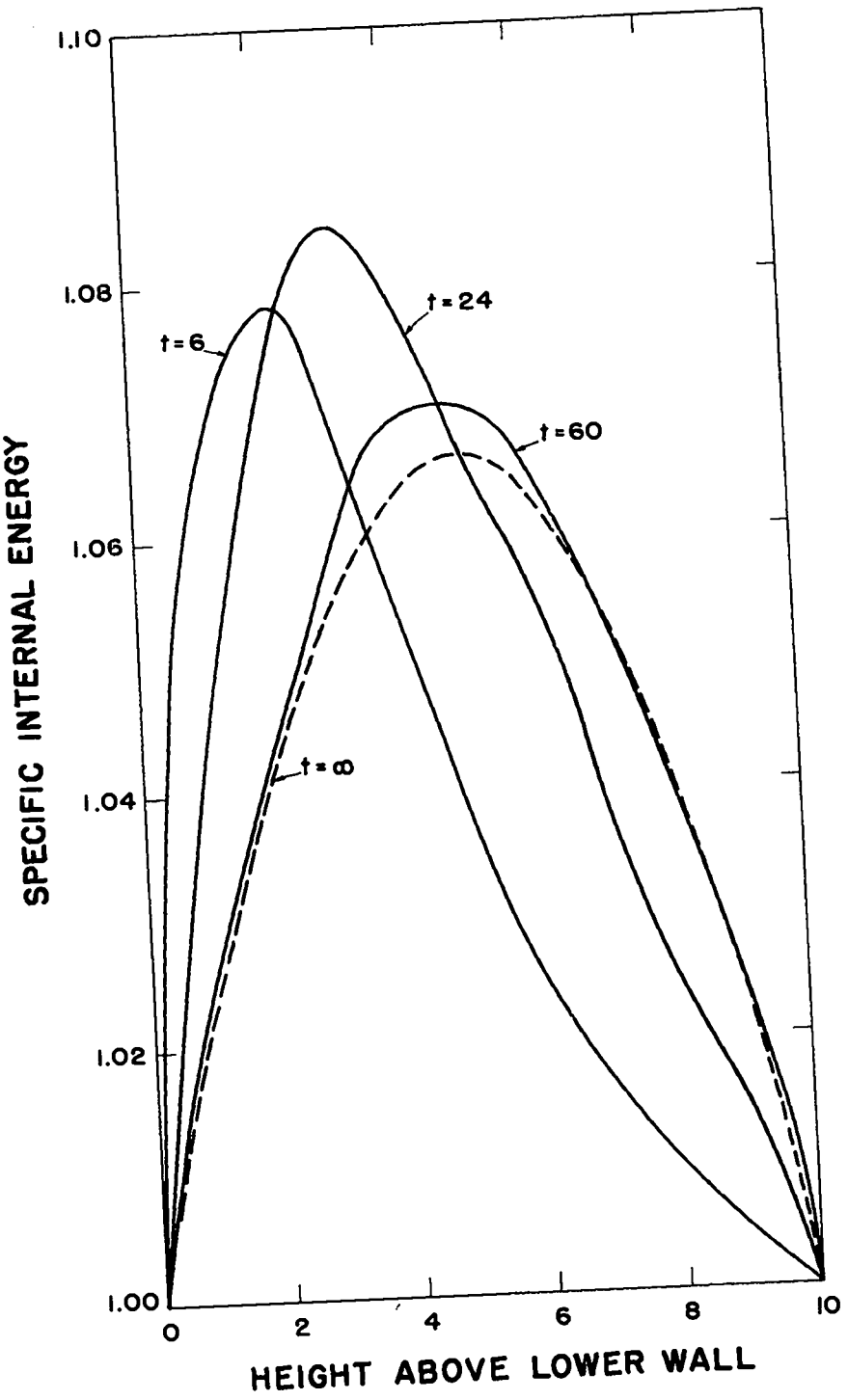

Fig. VII-2 Solid curves show machine-calculated specific internal energy as a function of height for low-velocity Couette flow. Dashed curve is analytical steady-state solution.

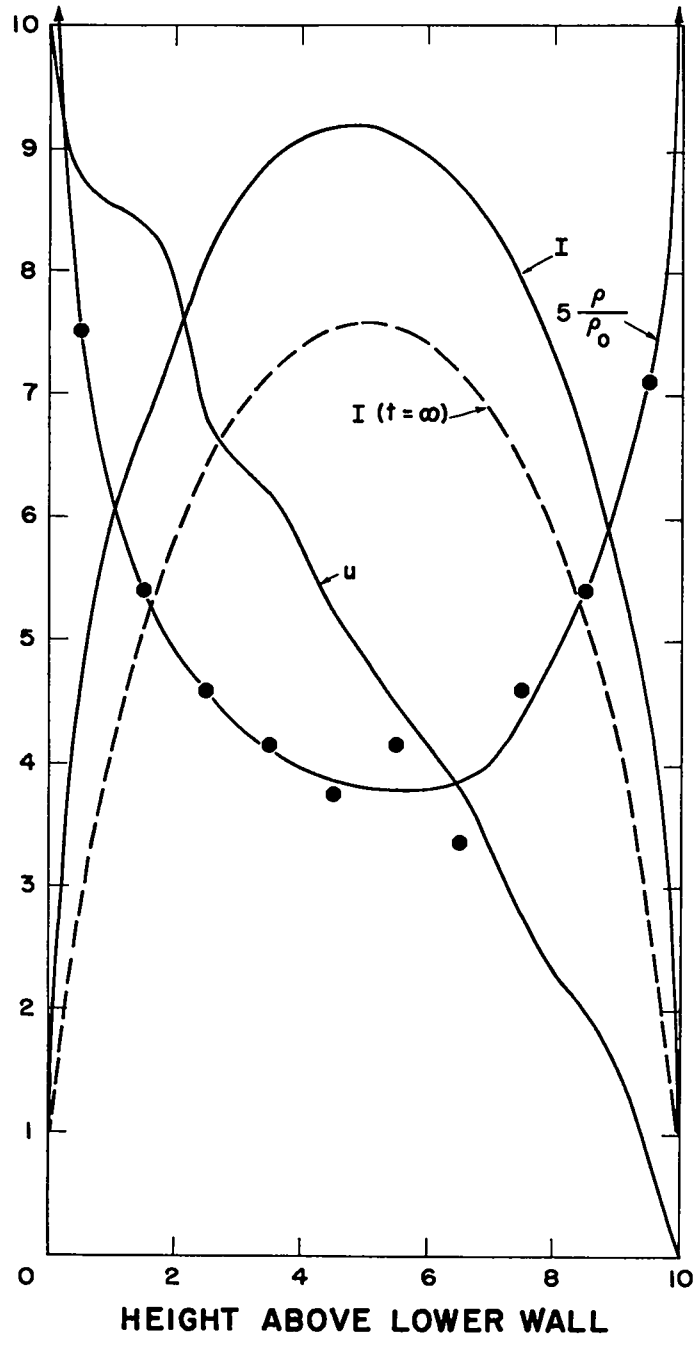

Fig. VII-3 Specific internal energy, velocity, and five times the compression plotted as functions of height for a high-velocity Couette flow calculation. Dashed curve is analytical steady-state solution. Points show the actual cellwise values of five times the compression.

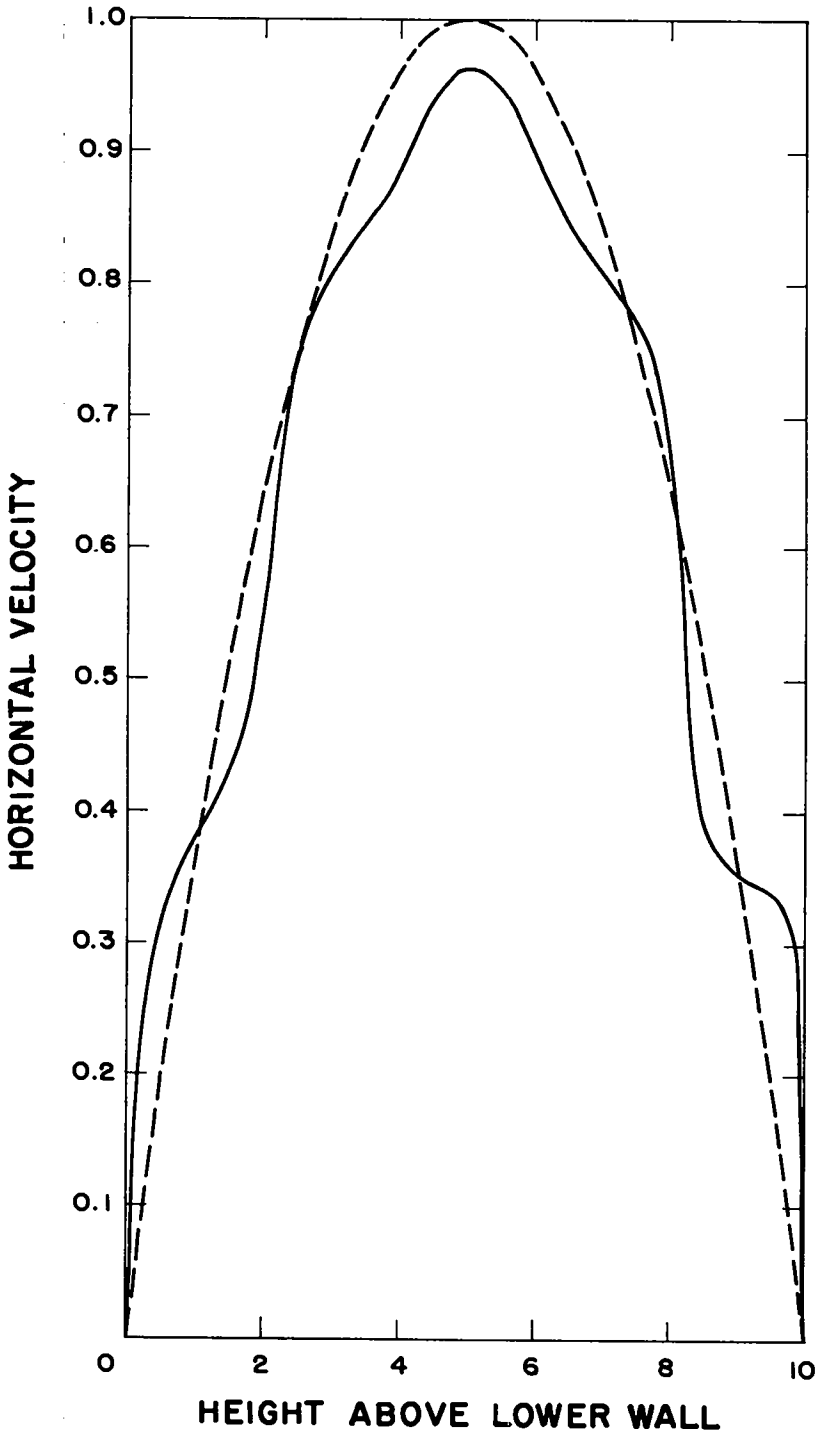

Fig. VII-4 Velocity as a function of height in the Poiseuille-flow problem. Solid curve is from machine calculation; dashed is analytical approximate solution.

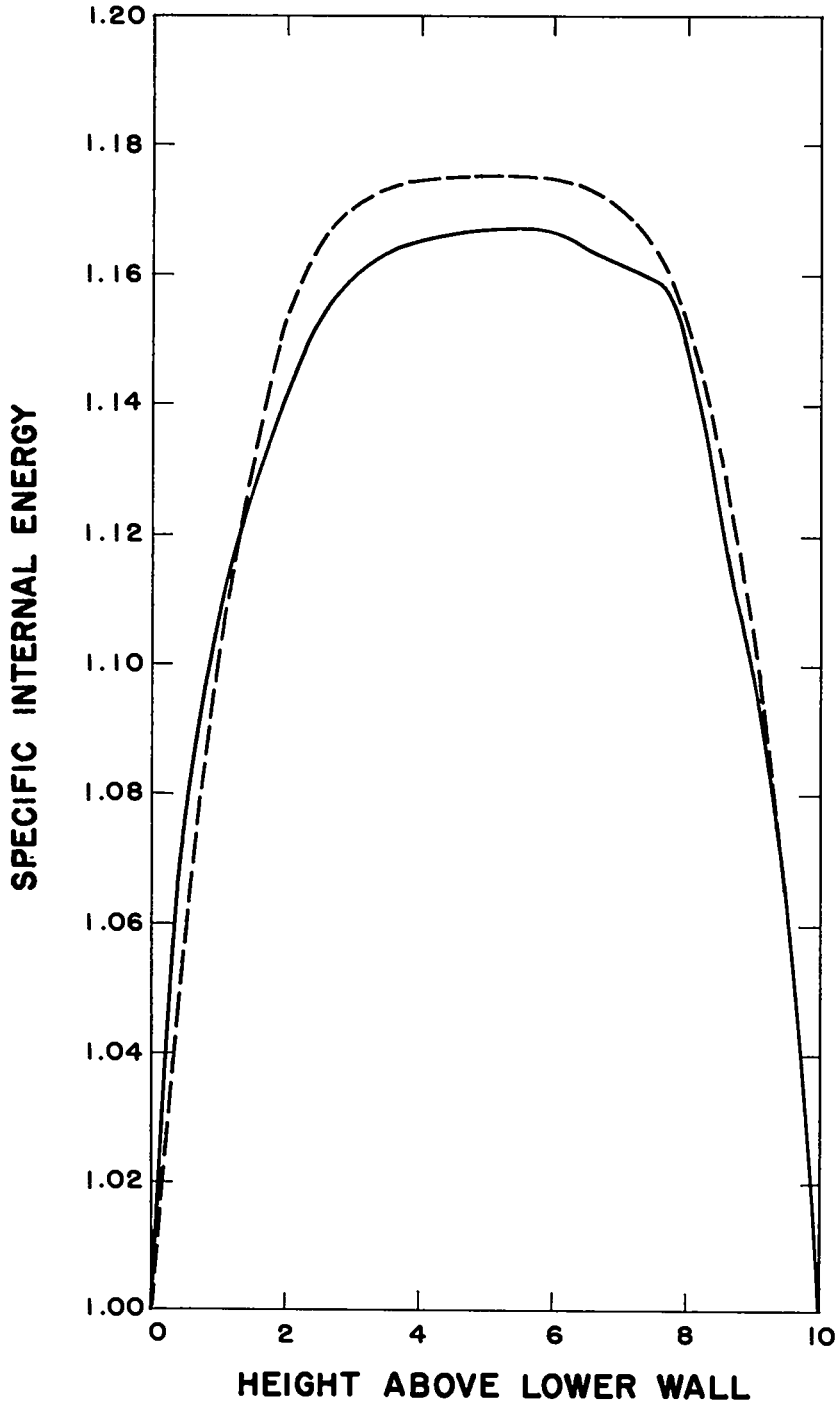

Fig. VII-5 Specific internal energy as a function of height in the Poiseuille-flow problem. Solid curve is from machine calculation; dashed is analytical approximate solution.

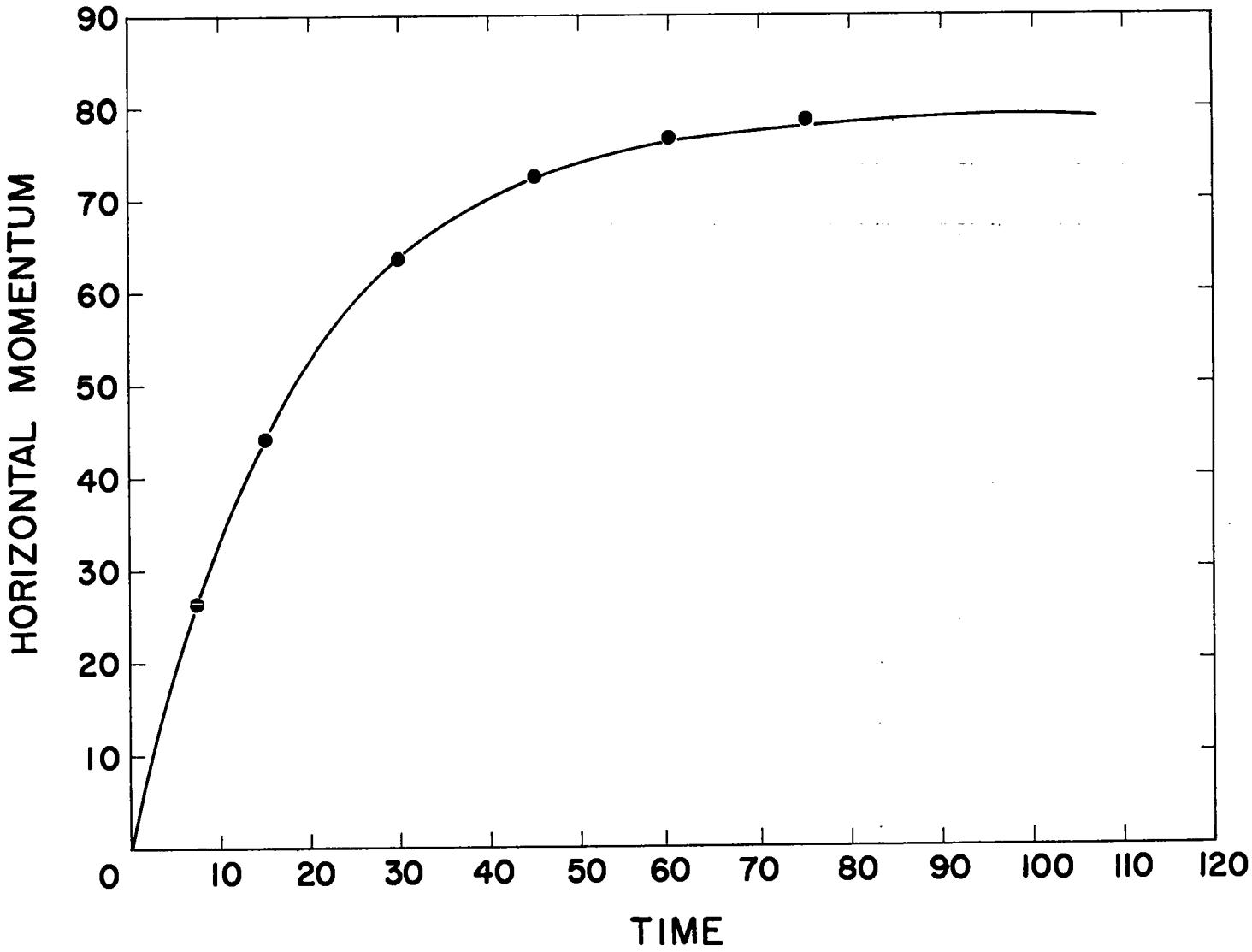

Fig. VII-6 Horizontal momentum as a function of time in the Poiseuille-flow problem. Solid curve is from machine calculation; datum points are analytical approximate solution.

REFERENCES

1. Harlow, F. H., and Evans, M. W., "Machine Calculation Method for Hydrodynamic Problems," Los Alamos Scientific Laboratory Report LAMS-1956, Nov. 23, 1955. (Not available, see LA-2139.)

2. Harlow, F. H., Evans, M. W., and Harris, D. E., Jr., "The Particle-in-Cell Method for Two-Dimensional Hydrodynamic Problems," Los Alamos Scientific Laboratory Report LAMS-2082, Aug. 29, 1956. (Not available, see LA-2139.)

3. Harlow, F. H., "Hydrodynamic Problems Involving Large Fluid Distortions," J. Assoc. Comp. Mach., 4, 137, April, 1957.

4. Evans, M. W., and Harlow, F. H., "The Particle-in-Cell Method for Hydrodynamic Calculations," Los Alamos Scientific Laboratory Report LA-2139, June 1957.

5. Evans, M. W., and Harlow, F. H., "Calculation of Supersonic Flow Past an Axially Symmetric Cylinder," J. Aeronaut. Sci., 25, 269 (1958).

6. Harlow, F. H., and Dickman, D. O., "Numerical Study of the Motions of Variously-Shaped Slabs Accelerated by a Hot Gas," Los Alamos Scientific Laboratory Report LA-2256, Sept. 1958.

7. Evans, M. W., and Harlow, F. H., "Calculation of Unsteady Flow Past a Circular Cylinder," J. Am. Rocket Soc., 29, 46 (1959).

8. Longley, H. J., personal communication.

9. Jahn, R. G., "The Refraction of Shock Waves at a Gaseous Interface," J. Fluid Mech., 1, 457 (1956).

10. Polachek, H., and R. J. Seeger, "On Shock-Wave Phenomena; Refraction of Shock Waves at a Gaseous Interface," Phys. Rev. 84, 922 (1951).

11. Jahn, R. G., "The Refraction of Shock Waves at a Gaseous Interface," Princeton University, Department of Physics, Technical Reports: #II-16, "Regular Refraction of Weak Shocks," June, 1954; #II-18, "Regular Refraction of Strong Shocks," February, 1955; #II-19, "Irregular Refraction," April, 1955.

12. Taub, A. H., "Refraction of Plane Shock Waves," Phys. Rev. 72, 51 (1947).

13. Whitham, G. B., "A New Approach to Problems of Shock Dynamics, Part I, Two-Dimensional Problems," J. Fluid Mech., 2, 145 (1957).

14. Laporte, O., "On the Interaction of a Shock with a Constriction," Los Alamos Scientific Laboratory Report LA-1740, August, 1954.